



OPEN

## Synthesis and application of [Zr-UiO-66-PDC-SO<sub>3</sub>H]Cl MOFs to the preparation of dicyanomethylene pyridines via chemical and electrochemical methods

Amir Mohammad Naseri<sup>1</sup>, Mahmoud Zarei<sup>1</sup>, Saber Alizadeh<sup>1</sup>, Saeed Babaei<sup>1</sup>, Mohammad Ali Zolfigol<sup>1</sup>, Davood Nematollahi<sup>1</sup>, Jalal Arjomandi<sup>1</sup> & Hu Shi<sup>2</sup>

A metal–organic framework (MOF) with sulfonic acid tags as a novel mesoporous catalyst was synthesized. The precursor of Zr-UiO-66-PDC was synthesized both via chemical and electrochemical methods. Then, zirconium-based mesoporous metal–organic framework [Zr-UiO-66-PDC-SO<sub>3</sub>H]Cl was prepared by reaction of Zr-UiO-66-PDC and SO<sub>3</sub>HCl. The structure of [Zr-UiO-66-PDC-SO<sub>3</sub>H]Cl was confirmed by FT-IR, PXRD, FE-SEM, TEM, BET, EDX, and Mapping analysis. This mesoporous [Zr-UiO-66-PDC-SO<sub>3</sub>H]Cl was successfully applied for the synthesis of dicyanomethylene pyridine derivatives via condensation of various aldehyde, 2-aminoprop-1-ene-1,1,3-tricarbonitrile and malononitrile. At the electrochemical section, a green electrochemical method has successfully employed for rapid synthesis of the zirconium-based mesoporous metal–organic framework UiO-66-PDC at room temperature and atmospheric pressure. The synthesized UiO-66-PDC has a uniform cauliflower-like structure with a 13.5 nm mean pore diameter and 1081.6 m<sup>2</sup> g<sup>-1</sup> surface area. The described catalyst [Zr-UiO-66-PDC-SO<sub>3</sub>H]Cl was also employed for the convergent paired electrochemical synthesis of dihydropyridine derivatives as an environmentally friendly technique under constant current at 1.0 mA cm<sup>-2</sup> in an undivided cell. The proposed method proceeds with moderate to good yields for the model via a cooperative vinylogous anomeric based oxidation.

Functionalized metal–organic frameworks (MOFs) are crystalline structures composed of suitable organic ligands and metal centers<sup>1</sup>. So far, these materials have been applied such as catalyst<sup>2</sup>, adsorbents and so on<sup>3,4</sup>. Ionic liquids-like MOFs (IL@MOFs) as novel homolog porous materials are some useful properties such as non-flammability, high thermal and chemical stability. Therefore, the joining of ionic liquids (ILs) and metal–organic frameworks (MOFs) as novel materials have been used as catalysts, gas adsorption and reagents<sup>5,6</sup>. This strategy have been modified to adjust to physical or chemical properties, pore size, surface area, topology, and polarity of IL@MOFs by suitable choice of metal, ligands and other moieties.

Zirconium is widespread in nature and used in biological systems. Firstly Zr-based metal–organic frameworks (Zr-MOFs) by Lillerud et al. in 2008 was prepared and reported<sup>7</sup>. Zr-MOFs has higher thermal stability and outstanding chemical stability in solvent and air<sup>8</sup> than other M-MOFs (M = metal) which made them applicable for industrial process and organic synthesis. Topology or morphology of Zr-MOFs are such as Fcu, Csq, Ftw, Bct, Spn, Sqc and etc.<sup>9–12</sup>. Topology of Zr-UiO-66-PDC as one of the precursors for the preparation of the presented [Zr-UiO-66-PDC-SO<sub>3</sub>H]Cl have been studied<sup>13</sup>.

Ionic liquids with N–S bonds have been introduced by Zolfigol et al. in 2011<sup>14</sup>. These materials have been applied as catalysts, reagents and solvents in the synthesis of a wide range of organic compounds<sup>15,16</sup>. In 2013, 1-sulfonypyridinium chloride [pyridine-SO<sub>3</sub>H]Cl has been synthesized by reaction of chlorosulfonic acid and

<sup>1</sup>Faculty of Chemistry, Bu-Ali-Sina University, 65174-38683 Hamedan, Iran. <sup>2</sup>School of Chemistry and Chemical Engineering, Institute of Molecular Science, Shanxi University, Taiyuan 030006, China. ✉email: mahmoud8103@yahoo.com; s.alizade66@yahoo.com; zolfi@basu.ac.ir; nemat@basu.ac.ir

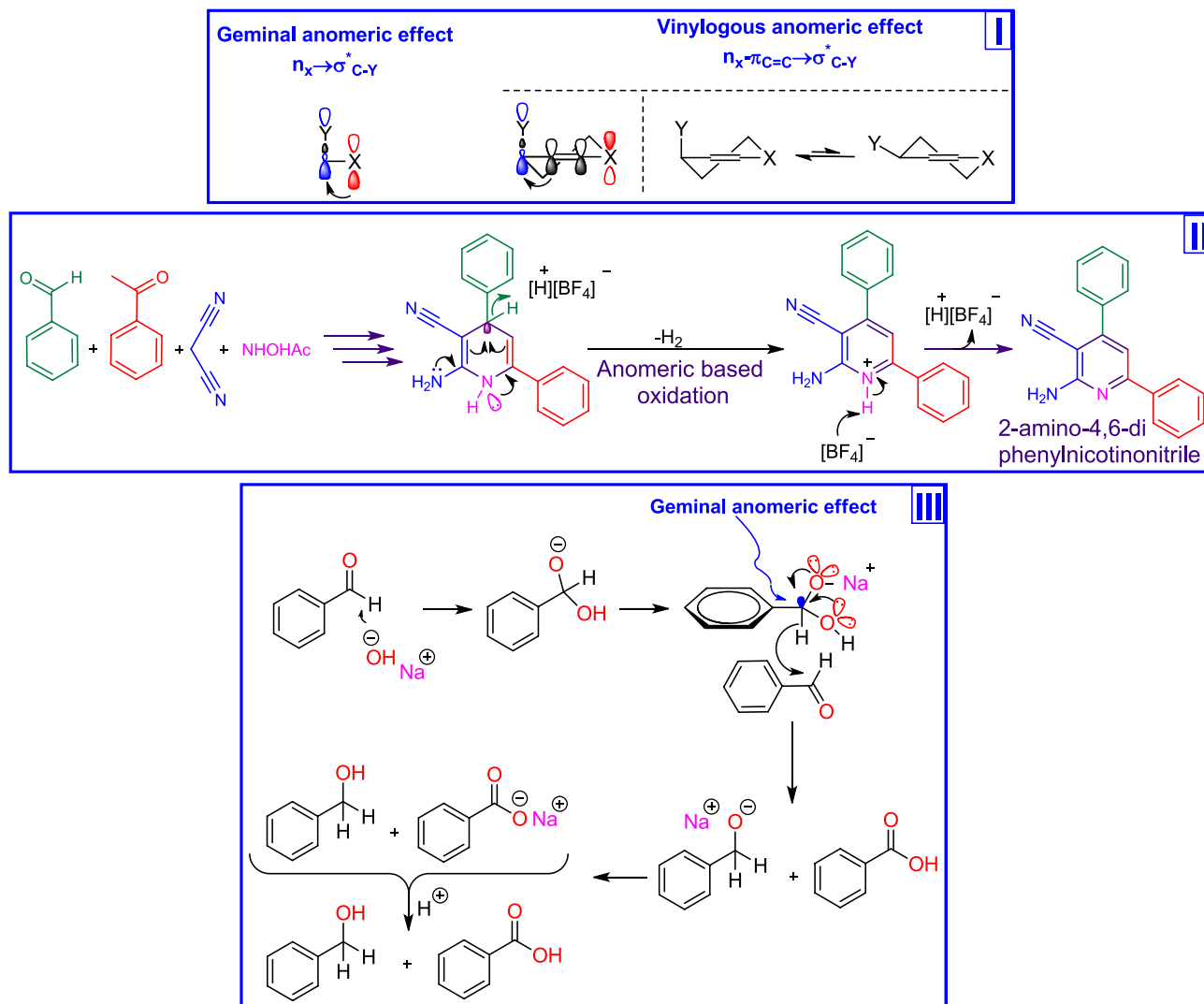


**Figure 1.** Part I: Geminal versus vinylogous anomeric effect. Part II: A cooperative vinylogous anomeric based oxidation leads to the preparation of 2-amino-4,6-diphenylnicotinonitrile<sup>37</sup>. Part III: A cooperative geminal anomeric based oxidation leads to hydride transfer in the mechanism of Cannizzaro reaction<sup>38</sup> (CambridgeSoft).

pyridine (1:1) at 0 °C, which have been applied for the synthesis of other ILs with other anions via anion exchange methods<sup>15–18</sup>. To combined metal–organic frameworks (MOFs) and ionic liquids (ILs), we have reacted Zr–UiO-66-PDC and  $ClSO_3H$  for preparing  $[Zr-UiO-66-PDC-SO_3H]Cl$  as a novel porous catalyst.

In recent years, many efforts have been made to investigate the biological properties pyridine and its derivatives. Therefore, it is very important to provide novel and easy strategies for the synthesis of target molecules with specific properties. In this regard, pyridines and 1,4-dihydropyridines are suitable candidates for biological and pharmacological studies<sup>19,20</sup>. These compounds have been applied as drugs for cancer, malaria, HIV, antimicrobial, anti-tumour, antifungal, anticonvulsant, antihypertension and urinary incontinence treatment<sup>19–27</sup>.

On the other hand, chemical reactivity is very complex. Numerous factors control the reaction mechanisms which are subject to everyday experiences. According to the alabugin's theory, one of the most effective factors is stereoelectronic effects, which are the stabilizing interactions of orbitals in space, are based on the quantum nature of molecular bonding but express this nature in a set of simple and intuitive practical rules that build a bridge between structure and reactivity<sup>28,29</sup>. Anomeric effect (AE) has been divided to different kinds such as geminal (Endo, Exo and reverse), vinylogous and so on (Fig. 1, Part I)<sup>28</sup>.

The relationship and detail of the impact of AE as an oldest stereoelectronic effect on structure and reactivity is also our main interest. This paper attempts to describe the role of vinylogous AE in the course of the synthesis of target molecules. Recently, we have introduced and developed a new term entitled “anomeric based oxidation” (ABO) in the course of special reactions<sup>30–36</sup>. Cooperative geminal and vinylogous ABO has been reviewed (Fig. 1, Parts II and III)<sup>37,38</sup>. Behind the chemical studies, many efforts have been done to access a mild and green condition for the electrocatalysis and application of MOFs<sup>39–50</sup>. Anodic and cathodic electrocatalysis methods are the important techniques that recently have been used for the preparation of various kinds of MOFs<sup>39–44</sup>. Even though the significant chemical<sup>51–53</sup> and electrochemical synthesis<sup>54–56</sup> of Zr based MOFs have been dedicated

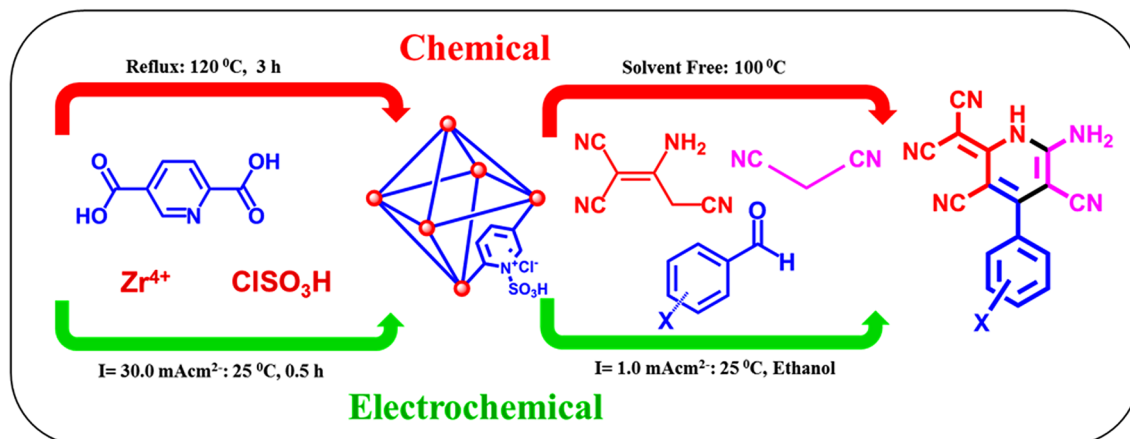


**Figure 2.** Synthesis of dicyanomethylene pyridines using [Zr-UiO-66-PDC-SO<sub>3</sub>H]Cl as a catalyst by chemical (A) and electrochemical (B) methods.

to the UiO-66 MOF, there are not any reports using cathodic electrosynthesis of UiO-66 derivatives at room temperature and pressure.

In this work, we wish to report the electrosynthesis of the mesoporous UiO-66-PDC (Zr-mMOF) via a reductive electrosynthesis technique as the first example. It was found that the electrosynthesis of Zr-mMOF by this method is rapid and could be done at room temperature and pressure without the need for any base or pre-base additive for activation of the ligand.

These results proved by the Fourier Transforms Infrared (FT-IR) spectroscopy, Field Emission Scanning Electron Microscopy (FE-SEM) and N<sub>2</sub> adsorption–desorption isotherm. At the second step and after treatment of electro-synthesized UiO-66-PDC by the SO<sub>3</sub>HCl, the catalyst, [Zr-UiO-66-PDC-SO<sub>3</sub>H]Cl was employed in a green procedure for convergent paired electrosynthesis of dihydropyridine compounds. “Paired electrosynthesis” have been successfully employed for the synthesis of organic and inorganic compounds<sup>40,57–59</sup>. This positive glance comes from the improved energy efficiency, enhanced atom economy, time-saving, and increasing electrochemical yield<sup>60–63</sup>. We imagined that the convergent pairing of two electrochemical reactions would provide a promising protocol towards the green chemistry principles. In other words, by the implementation of this strategy, cooperative anodic and cathodic reactions lead to a one-step process at green solvent and room temperature and without the need for any ex-situ base additive and replacement of the electrodes.

According to the above concepts, after preparation of Zr-metal–organic frameworks [Zr-UiO-66-PDC-SO<sub>3</sub>H]Cl as a mesoporous catalyst, it was employed for the synthesis and electrosynthesis of special dicyanomethylene pyridines by condensation of various aldehydes (bearing electron-donating and electron-withdrawing groups), malononitrile and 2-aminoprop-1-ene-1,1,3-tricarbonitrile under solvent-free conditions at 100 °C (method A) and constant current electrolysis via the convergent paired electrosynthesis in the ethanol at room temperature and pressure (method B) (Fig. 2).

## Results and discussion

Nowadays inter and multidisciplinary researches and investigations are a great demand both for academics and industries researchers. On the other hand, making bridges between basic to advanced concepts are necessary for the development of knowledge. In this research, chemical and electrochemical methods for the preparation of designed molecules were applied. Stereoelectronic effects as a bridge between structure and reactivity was also considered in the course of reactions<sup>28</sup>. With this aim, we have studied reactions and the obtained results are presented.

**Chemical and electrochemical preparation of Zr-mMOF.** Metal–organic frameworks (MOFs) based on Zr is attractive groups for preparing catalysts and/or reagents. Herein, we attempt to the preparation of Zr-UiO-66-PDC with sulfonic acid groups. For this purpose, we prepared Zr-UiO-66-PDC via H<sub>2</sub>PDC and ZrCl<sub>4</sub><sup>13</sup>. Then, [Zr-UiO-66-PDC-SO<sub>3</sub>H]Cl was prepared as ionic liquid transported into Zr-UiO-66-PDC. The structure of mentioned ionic liquid transported into Zr-MOFs, [Zr-UiO-66-PDC-SO<sub>3</sub>H]Cl, fully was characterized by applying FT-IR, XRD, BET/BJH, TG, DTG, EDX, FE-SEM as well as TEM analysis.

The FT-IR spectrum of pyridine-2,5-dicarboxylic acid (H<sub>2</sub>PDC), ZrCl<sub>4</sub>, Zr-UiO-66-PDC and [Zr-UiO-66-PDC-SO<sub>3</sub>H]Cl were compared in Fig. 3. The broad peak of O–H stretching related to SO<sub>3</sub>H group at 2700–3500 cm<sup>-1</sup> and peaks observed at 1186 and 1063 cm<sup>-1</sup> were related to stretching O–S and N–S respectively<sup>16</sup>. The peak 1733 cm<sup>-1</sup> in H<sub>2</sub>PDC was related to stretching C=O bond. Also, the PXRD pattern indicates the crystallinity of synthesized [Zr-UiO-66-PDC-SO<sub>3</sub>H]Cl (Fig. 3)<sup>13</sup>.

The materials in the structure of [Zr-UiO-66-PDC-SO<sub>3</sub>H]Cl and Zr-UiO-66-PDC were characterized by energy-dispersive X-ray spectroscopy (EDX) (Fig. 4). The [Zr-UiO-66-PDC-SO<sub>3</sub>H]Cl has confirmed the existence of Zr, C, O, S, Cl and N atoms whereas the structure of Zr-UiO-66-PDC which is contained Zr, C, N and O atoms. Furthermore, the well-dispersed distribution of elements in the [Zr-UiO-66-PDC-SO<sub>3</sub>H]Cl was determined and

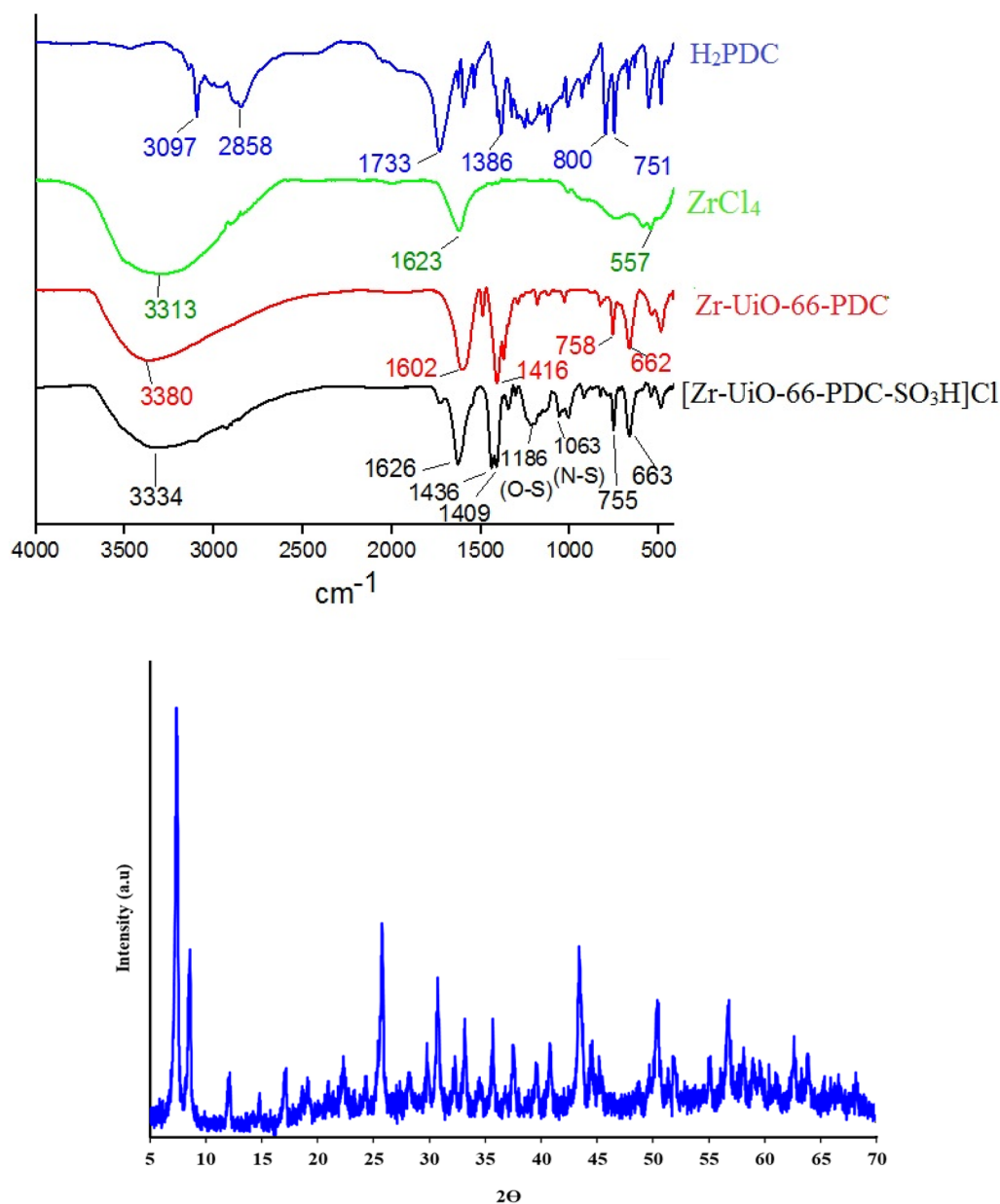


**Figure 3.** Up: FT-IR spectra of pyridine-2,5-dicarboxylic acid ( $\text{H}_2\text{PDC}$ ),  $\text{ZrCl}_4$ ,  $\text{Zr-UiO-66-PDC}$  and  $[\text{Zr-UiO-66-PDC-SO}_3\text{H}]\text{Cl}$ . Down: PXRD pattern of the  $[\text{Zr-UiO-66-PDC-SO}_3\text{H}]\text{Cl}$ .

verified by elemental mapping (Fig. 4). The difference between FT-IR, EDX and SEM-elemental mapping of  $\text{Zr-UiO-66-PDC}$  and  $[\text{Zr-UiO-66-PDC-SO}_3\text{H}]\text{Cl}$  vouched for the structure of target Zr-MOFs.

In another investigation, the topography of  $[\text{Zr-UiO-66-PDC-SO}_3\text{H}]\text{Cl}$  was examined by scanning electron microscopy (SEM) images. As shown in Fig. 5, topography particles of the catalysts are fcu which are in good agreement and not completely accumulated. In addition, the topography structure of  $[\text{Zr-UiO-66-PDC-SO}_3\text{H}]\text{Cl}$  was studied more closely using transmission electron microscopy (TEM) micrograph in Fig. 5. Therefore,  $[\text{Zr-UiO-66-PDC-SO}_3\text{H}]\text{Cl}$  are fcu topological network with 12-connected Zr clusters.

In order investigation, the structural and thermal stability of  $[\text{Zr-UiO-66-PDC-SO}_3\text{H}]\text{Cl}$  was also determined using the technique of the thermal gravimetric (TG), derivative thermal gravimetric (DTG), as well as differential thermal analysis (DTA) (Fig. 6). Initial stage weight loss is between room temperature up to  $100\text{ }^\circ\text{C}$ , associated with organic solvents and  $\text{H}_2\text{O}$  which have been applied in the course of preparation of  $[\text{Zr-UiO-66-PDC-SO}_3\text{H}]\text{Cl}$ . In continued, twice steps of weight loss (includes about 30% weight loss) has occurred at about  $300\text{ }^\circ\text{C}$  which is linked to breaking the band of N-S of the structure of the catalyst. Therefore, according to literature survey<sup>13</sup>, the structure of  $[\text{Zr-UiO-66-PDC-SO}_3\text{H}]\text{Cl}$  is stable, even after adding sulfonic acidic functional groups.

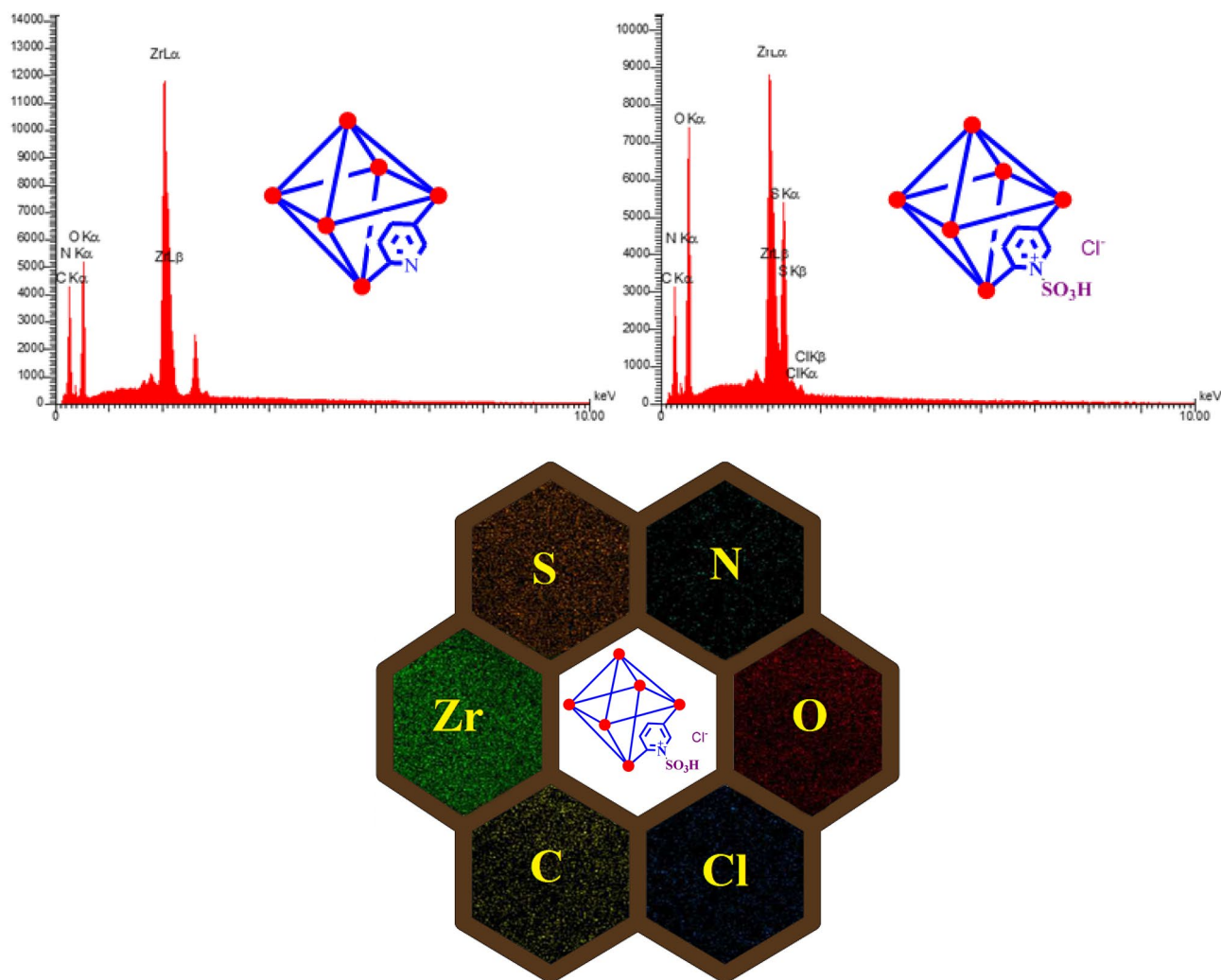


**Figure 4.** Up: Energy-dispersive X-ray spectroscopy (EDX) of  $[\text{Zr-UiO-66-PDC-SO}_3\text{H}]\text{Cl}$  and  $\text{Zr-UiO-66-PDC}$ . Down: Elemental mapping analysis of  $[\text{Zr-UiO-66-PDC-SO}_3\text{H}]\text{Cl}$ . The structures of the compounds were drawn using Chem Office 12.0 (Cambridge Soft).

Features of the prepared functionalized MOFs such as Surface area, pore volumes and pore size distribution were obtained using  $\text{N}_2$  adsorption–desorption isotherm (Fig. 6). The calculated surface areas using the BET equation, total pore volume and average pore size are  $15.24 \text{ m}^2 \text{ g}^{-1}$ ,  $0.1914 \text{ cm}^3 \text{ g}^{-1}$  and  $50.22 \text{ nm}$  respectively.

We also employed a cathodic (reductive) electrochemical technique for the preparation of  $\text{Zr-UiO-66-PDC}$ . As shown in Fig. 7. Our procedure involves immersing a carbon electrode in a solution containing pyridine-2,5-dicarboxylic acid ( $\text{H}_2\text{PDC}$ ) as a ligand, zirconium tetrachloride as a cation source and potassium nitrate as a supporting electrolyte. In-situ electrogeneration of hydroxide ions generated by electroreduction of water (as a co-solvent),  $\text{NO}_3^-$  (as a counter ion) and/or direct deprotonation of ligand at  $30.0 \text{ mA cm}^{-2}$  for 1800s is an essential requirement in this method<sup>39–42,44</sup>. An increase in the local pH at the cathode surface causes activation of the ligands (deprotonation), and consequently formation of  $\text{Zr-UiO-66-PDC}$  through the coordination of activated ligands with zirconium cations (Fig. 7)<sup>55,56</sup>. The nucleation rate and growth of  $\text{Zr-UiO-66-PDC}$  are only controlled by the cathodic reaction without the need for any ex-situ base/probes additive, at room temperature, atmospheric pressure, and short time.

Characterization of the prepared  $\text{Zr-UiO-66-PDC}$  was examined by the FT-IR, PXRD, FE-SEM, BET, EDX and mapping analysis. To confirm the functionality and bonding groups of the electrosynthesized  $\text{UiO-66-PDC}$  MOF, FT-IR analysis was performed. The obtained pattern is consistent with the reported pattern of chemical procedure<sup>13</sup> (Fig. 8A). Also, the recorded PXRD pattern proved the purity and high crystallinity of the electrosynthesized  $\text{Zr-UiO-66-PDC}$  MOF that is consistent with the reported pattern<sup>13</sup> and the  $\text{Zr}$  based MOFs synthesized by electrochemical method<sup>55,56</sup> (Fig. 8B). FE-SEM images of electrosynthesized ( $\text{UiO-66-PDC}$ ) under constant current conditions shows the uniform cauliflower-shaped nanoparticles with an average diameter size of around  $25.0 \text{ nm}$  (Fig. 8C). This result is consistent with the  $\text{Zr}$  based MOFs synthesized by electrochemical method<sup>55,56</sup>. The  $\text{N}_2$  adsorption/desorption isotherm of  $\text{Zr-UiO-66-PDC}$  is shown in Fig. 8D. A “type IV” isotherm with a hysteresis loop (between  $p/p_0 = 0.4$  and 1) which is characteristic of mesoporous materials is observed.

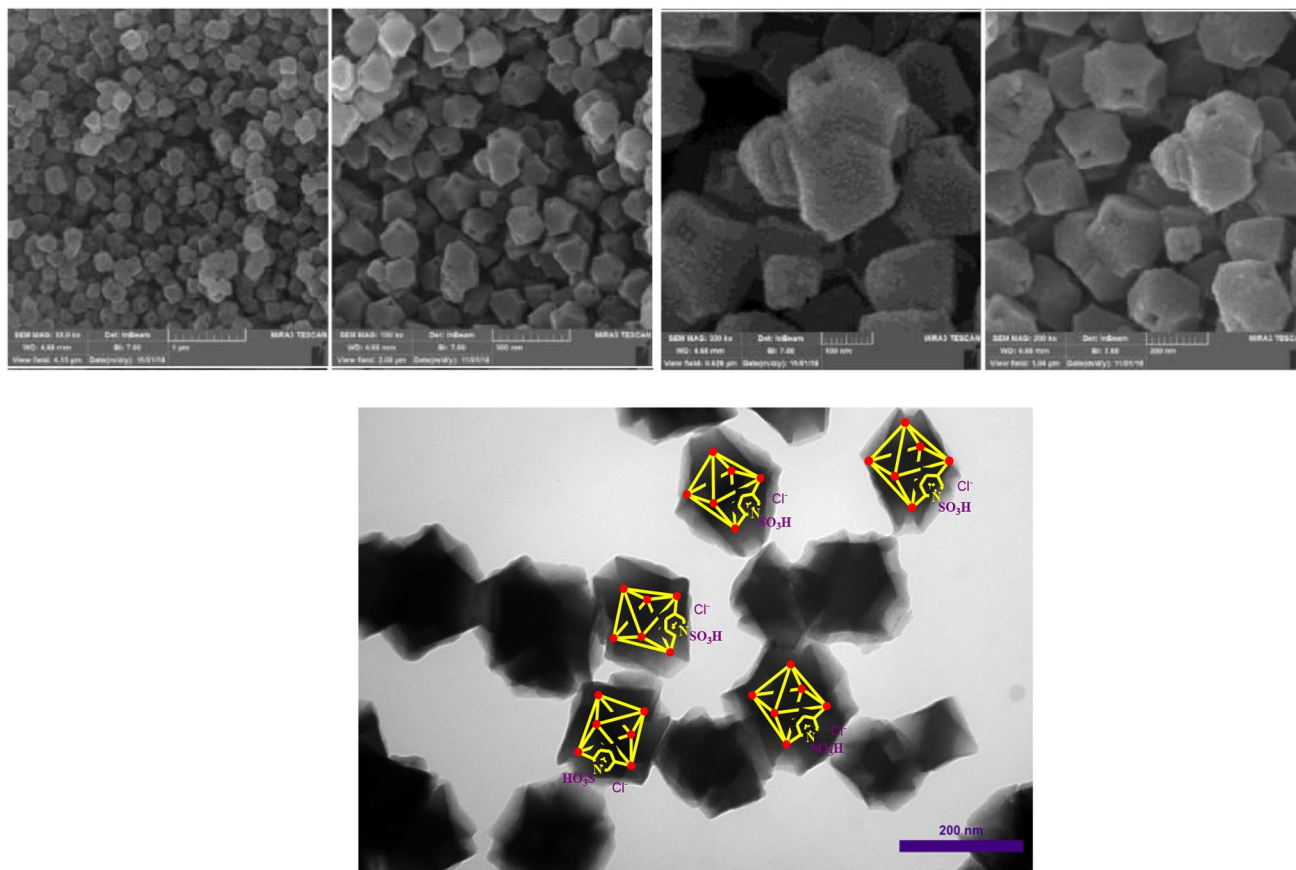


**Figure 5.** Up: Field-Emission Scanning electron microscopy (FE-SEM) images of  $[\text{Zr-UiO-66-PDC-SO}_3\text{H}]\text{Cl}$ . Down: Transmission electron microscopy (TEM) micrograph of  $[\text{Zr-UiO-66-PDC-SO}_3\text{H}]\text{Cl}$ .

Furthermore, the pore size distribution obtained by the Barrett-Joyner-Halenda (BJH) method shows two peaks of 1.2 and 18.9 nm but the average pore size is 13.4 nm. Besides, the specific surface area measured from the  $\text{N}_2$  isotherms is  $1081.6 \text{ m}^2 \text{ g}^{-1}$  that is higher than the obtained amount of above mentioned hydrothermal and microwave methods and is consistent with the Zr based MOFs prepared electrochemically<sup>55,56</sup>. Finally, the Zr-UiO-66-PDC structure was characterized by energy-dispersive X-ray spectroscopy (EDX) and mapping analysis (Fig. 8E). The obtained EDX pattern was confirmed the simultaneous existence of Zr, C, O, and N elements for the configuration of the Zr-UiO-66-PDC structure. Furthermore, mapping analysis was indicated the homogeneous and well-dispersed distribution of the above-mentioned elements in the Zr-UiO-66-PDC structure (Fig. 8E).

**Chemical and electrochemical synthesis of dicyanomethylene pyridine derivatives.** Lately, a wide range of dicyanomethylene pyridines was prepared via one-pot multi-component condensation reactions in the presence of a catalytic amount described  $[\text{Zr-UiO-66-PDC-SO}_3\text{H}]\text{Cl}$  as a mesoporous catalyst. The condensation of 4-chloro benzaldehyde, 2-aminoprop-1-ene-1,1,3-tricarbonitrile and malononitrile was selected as a model for optimization of the reaction conditions. As shown, the best condition reaction for the synthesis of 3,5-diaminobiphenyl-2,4,6-tricarbonitrile was achieved in the presence of 10.0 mg  $[\text{Zr-UiO-66-PDC-SO}_3\text{H}]\text{Cl}$  in refluxing water (Table 1 entry 10). Different amount of catalyst, temperature and solvent were not improved in the yield and time (Table 1 entries 1–17 except 10). The optimization of reaction conditions along with the isolated yields of products are summarized in Table 1.

After optimization reaction condition, the scope and limitations of  $[\text{Zr-UiO-66-PDC-SO}_3\text{H}]\text{Cl}$  as a novel catalyst was investigated in the preparation of dicyanomethylene pyridine via a condensation reaction of wide-spread analogue of aldehyde (mono, bis and tris substituted  $\text{C}=\text{O}$ ) which are bearing electron-donating and electron-withdrawing groups, malononitrile and 2-aminoprop-1-ene-1,1,3-tricarbonitrile.

As shown in Table 2, the results indicated that this strategy is appropriate for the synthesis of dicyanomethylene pyridine (Table 2). The proposed mechanism for the synthesis of dicyanomethylene pyridine derivatives using  $[\text{Zr-UiO-66-PDC-SO}_3\text{H}]\text{Cl}$  was summarized in Fig. 9. The  $\text{SO}_3\text{H}$  group of  $[\text{Zr-UiO-66-PDC-SO}_3\text{H}]\text{Cl}$  is activating the carbonyl group of aldehyde. In the first step, malononitrile is reacting with the carbonyl group of aldehyde to afford Knoevenagel's adduct I by removing one molecule of  $\text{H}_2\text{O}$ . Then, 2-aminoprop-1-ene-1,1,3-tricarbonitrile attacks to I to give intermediate II, which is reacting to give III via an intramolecular cyclocondensation. Finally, the intermediate III and IV was converted to the desired product VI through intermediate V via a cooperative vinylogous ABO and releasing one molecule of hydrogen ( $\text{H}_2$ ) (Fig. 9)<sup>31</sup>.

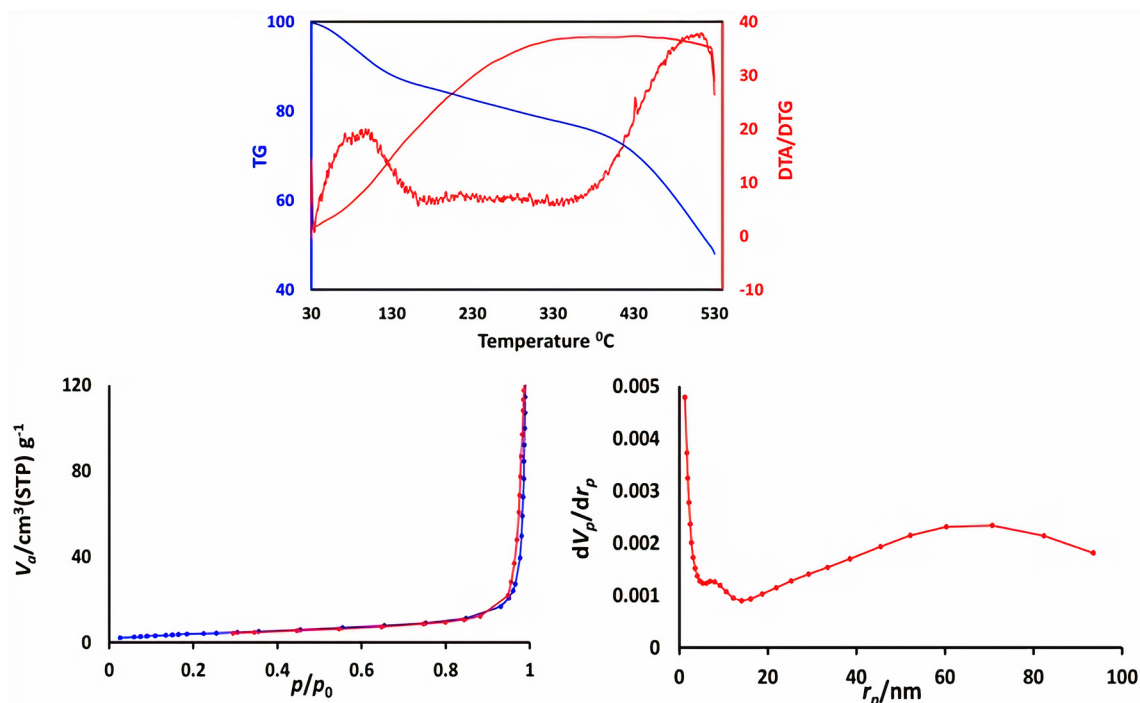


**Figure 6.** Up: TG, DTG and DTA analysis of [Zr-UiO-66-PDC-SO<sub>3</sub>H]Cl. This figure was prepared by Microsoft Excel (OFFICE 2013). Down: N<sub>2</sub> adsorption/desorption isotherm and pore size distribution (BJH) of [Zr-UiO-66-PDC-SO<sub>3</sub>H]Cl. This figure was prepared by Microsoft Excel (OFFICE 2013).

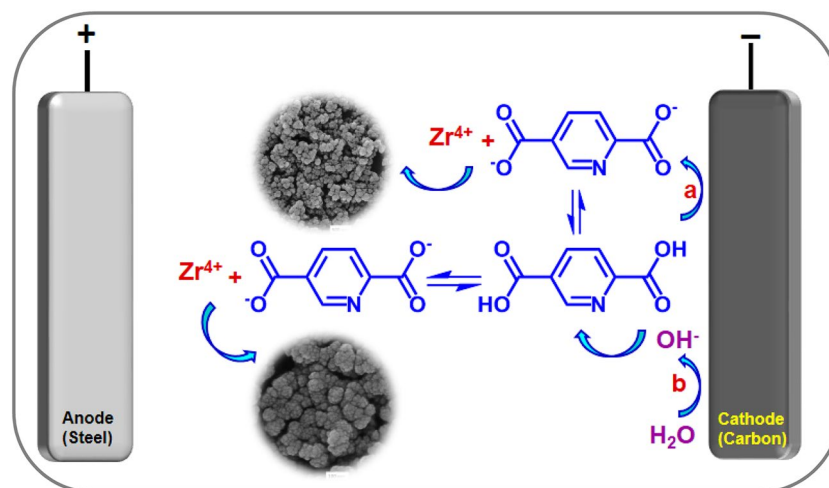


**Figure 7.** Electrochemical synthesis of (UiO-66-PDC) by constant current electrolysis at  $I = 30 \text{ mA cm}^{-2}$  and  $t = 1800 \text{ s}$ .

The obtained results from model reaction under argon and nitrogen atmospheres verified abovementioned our suggestion for the latter step. Literature survey shows that there is no rational and clear stepwise mechanism for synthesis of the presented molecules<sup>64,65</sup>. Herein, we wish to present a comprehensive mechanism for a mentioned reaction so that its final step might progress through a cooperative vinylogous ABO in the absence of oxygen molecules. In the intermediates III and IV, sharing the electron density from the Endo and Exo nitrogens lone pairs to the vacant antibonding  $\sigma^*$  orbital of  $\text{SP}^3$  C–H bond through vinylic C=C double bonds support the unusual hydride transfer for releasing the molecular hydrogen ( $\text{H}_2$ ). Recently, we have been named this phenomenon a new term entitled a cooperative vinylogous ABO and its development for various catalytic systems is our main research interest<sup>30–38</sup>. The described ABO mechanism is in good agreement with the "vinylogous anomeric effect" concept which at first, had been introduced by Katritzky<sup>66</sup>.

At the second step of this work, [Zr-UiO-66-PDC-SO<sub>3</sub>H]Cl was employed for the preparation of dihydropyridine compounds via convergent paired electrosynthesis as a green and sustainable technique. To shed light on

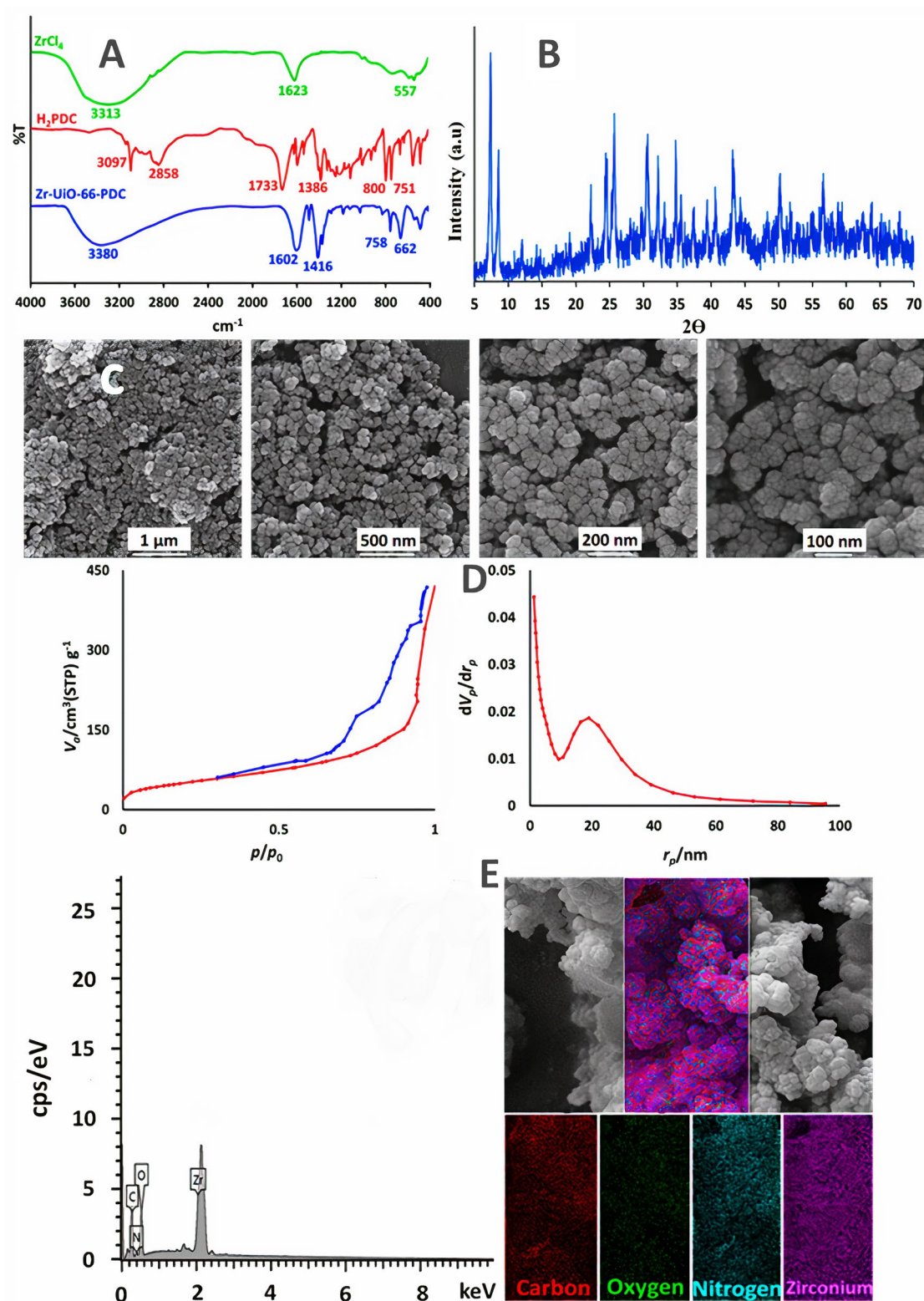
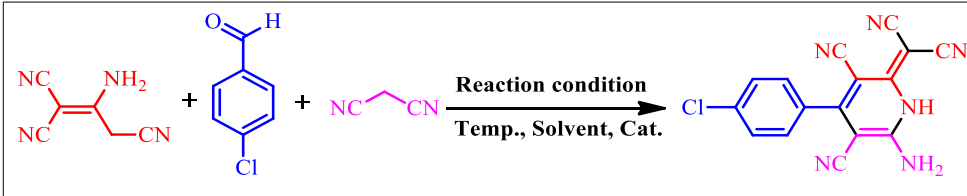


**Figure 8.** (A) FT-IR spectra of pyridine-2,5-dicarboxylic acid (H<sub>2</sub>PDC), ZrCl<sub>4</sub> and Zr-UiO-66-PDC. (B) Powder X-ray diffraction (PXRD) pattern of electro synthesized Zr-UiO-66-PDC. (C) Large- and close-view FE-SEM images of Zr-UiO-66-PDC by constant current electrolysis at  $I = 30 \text{ mA cm}^{-2}$  and  $t = 1800 \text{ s}$ . (D) N<sub>2</sub> adsorption/desorption isotherm. BET and BJH of Zr-UiO-66-PDC by the constant current electrolysis at  $I = 30 \text{ mA cm}^{-2}$  and  $t = 1800 \text{ s}$ . (E) Energy-dispersive X-ray spectroscopy (EDX) and elemental mapping analysis of electro synthesized Zr-UiO-66-PDC. The structures of the compounds were drawn using ChemOffice 12.0 (CambridgeSoft).





Entry	Solvent (5 mL)	Cat. (mg)	Temp. (°C)	Time (min)	Isolated yield (%)
1	DMF	10	100	120	38
2	EtOH	10	Reflux	120	60
3	CH <sub>2</sub> Cl <sub>2</sub>	10	Reflux	120	63
4	CHCl <sub>3</sub>	10	Reflux	120	20
5	EtOAc	10	Reflux	120	40
6	CH <sub>3</sub> CN	10	Reflux	120	58
7	PEG	10	Reflux	120	35
8	<i>n</i> -Hexane	10	Reflux	120	65
9	H <sub>2</sub> O	10	Reflux	120	52
10	–	10	100	20	87
11	–	5	100	30	75
12	–	15	100	30	87
13	–	20	100	30	85
14	–	10	25	120	15
15	–	10	50	120	68
16	–	–	75	120	10
17	–	10	100	120	70

**Table 1.** Effect of different amounts of catalyst, temperature and solvent (5.0 mL) in the synthesis dicyanomethylene pyridine.

this fact, as shown in Fig. 10, an undivided home-made cell comprising two electrodes under constant current electrolysis was employed for this purpose.

The convergent paired electrosynthesis was started by applying constant current electrolysis (CCE) ( $1.0 \text{ mA cm}^{-2}$ ) in ethanol and room temperature as green conditions. Upon the starting electrolysis, malononitrile can be activated to the methylene malononitrile on the cathodic electrode without the need for the ex-situ base additive. On the other hands, activation of the carbonyl group of aldehyde can be done by the  $\text{SO}_3\text{H}$  functional group of employed catalysis, simultaneously. So, the suitable condition for preparing the knoevenagel's adduct (I) will be provided through attacking the methylene malononitrile on the activated aldehyde and removing one  $\text{H}_2\text{O}$  molecule. At the second step, 2-aminoprop-1-ene-1,1,3-tricarbonitrile can be attacked to the in-situ prepared knoevenagel's adduct (I) via the Michael addition reaction.

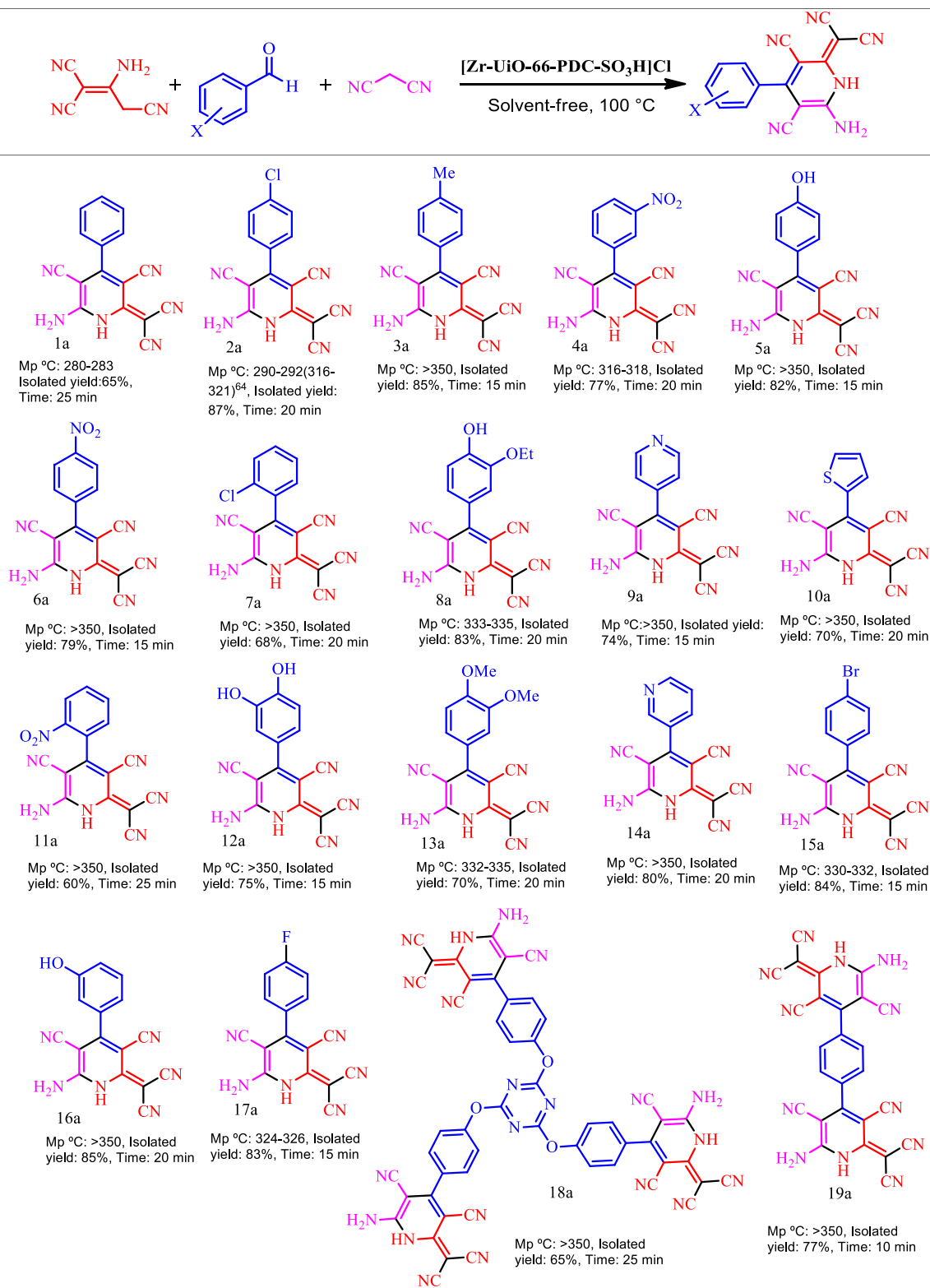
After tautomerization step (II), the produced intermediate (III) undergoes an intramolecular cyclocondensation by effective activation of nitrile functional group via  $\text{SO}_3\text{H}$  functional group of employed catalysis.

Finally, in order to the implementation and completing of the convergent paired electrosynthesis the produced intermediate (V) after tautomerization step (IV), can be oxidized on the anodic electrode by releasing two electron/two proton, in order to harvest the final product (VI). It should be noted, the progress and yield of a reaction in the absence of the  $[\text{Zr-UiO-66-PDC-SO}_3\text{H}]\text{Cl}$  catalyst were slow and low.

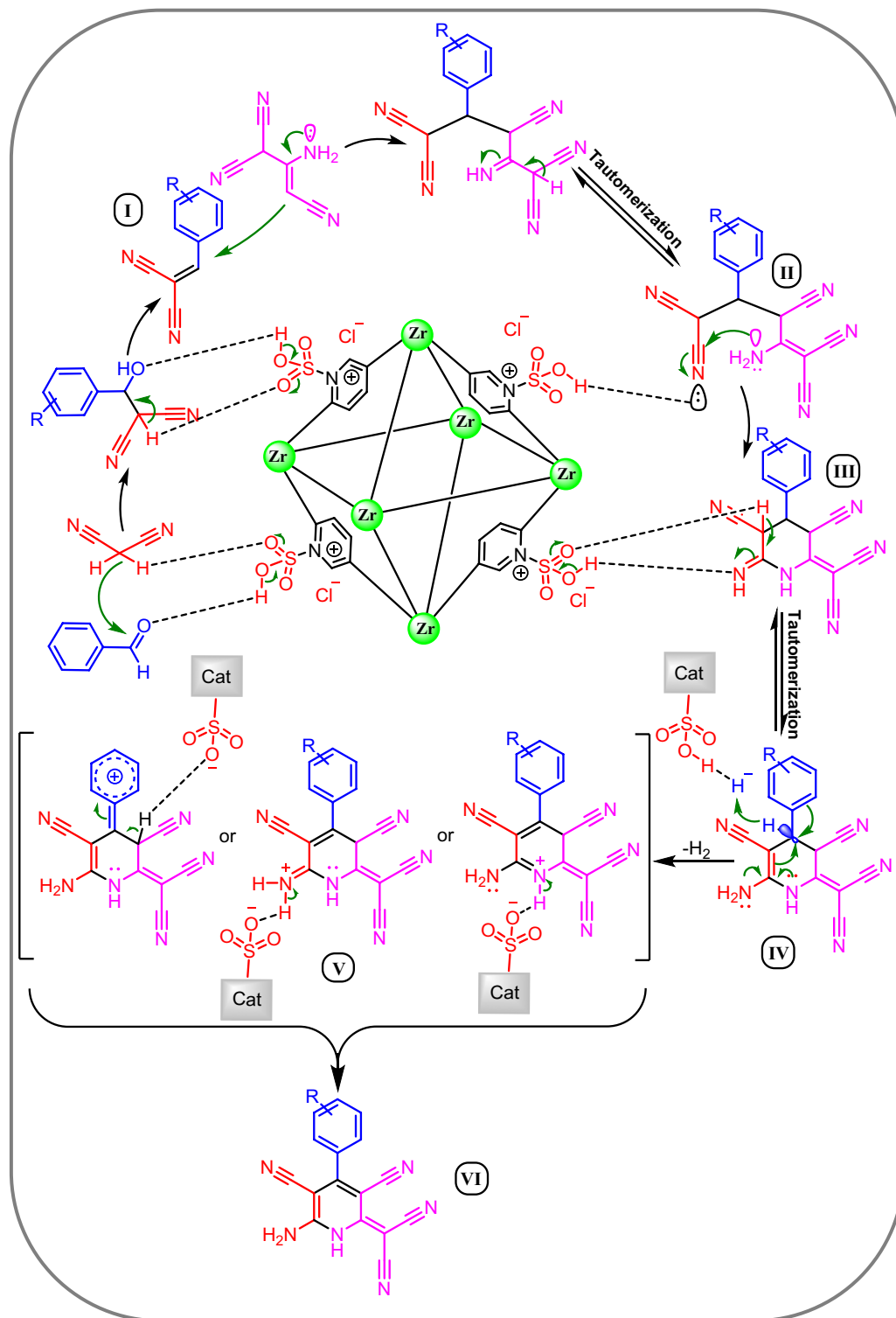
It is noteworthy to mention that, the higher applied currents lead to the occurrence of side reactions like polymerization of malononitrile and the lower applied currents lead to prolonged reaction time or low yields due to the inactivation of malononitrile. Table 3 indicate the optimization of applied current density at the electrolysis condition.

Table 4 indicates the results of the model reactions based on the electronic properties of substitute groups on the benzaldehyde. The data presented in Table 4 shows the applied procedure have a satisfying performance for electrosynthesis of related dihydropyridine derivatives in a one-pot reaction with a 63–85% overall yield. It is noteworthy to mention that, the higher product yield for aldehydes with electron-withdrawing groups, 4-Chlorobenzaldehyde, is comparable and even greater than that of their simple (benzaldehyde) and/or electron-donating (4-methylbenzaldehyde) group homologues. These results may be caused by more efficient deprotonation of related aldehydes bearing electron-withdrawing groups lead to an intermediate under the proposed mechanism. So, the obtained trend may be repeated for the other homologue aldehydes based on the electron characteristics of substituted groups with acceptable tolerance.

To evaluate the performance of  $[\text{Zr-UiO-66-PDC-SO}_3\text{H}]\text{Cl}$  as an efficient catalyst for the synthesis of dicyanomethylene pyridine, we have tested different acid catalysts (organic and inorganic) by reaction of 4-chloro benzaldehyde (1.0 mmol, 0.14 g), 2-aminoprop-1-ene-1,1,3-tricarbonitrile (1.0 mmol, 0.132 g), and malononitrile (1.1 mmol, 0.072 g) in Table 5. As a result in Table 5,  $[\text{Zr-UiO-66-PDC-SO}_3\text{H}]\text{Cl}$  is the best catalyst for the synthesis of dicyanomethylene pyridine.



**Table 2.** Effect of different amounts of catalyst, temperature and solvent (5.0 mL) in the synthesis dicyanomethylene pyridine.



**Figure 9.** A rational proposed mechanism for the synthesis of dicyanomethylene pyridine using [Zr-UiO-66-PDC-SO<sub>3</sub>H]Cl.

The results of catalytic activity and reusability of [Zr-UiO-66-PDC-SO<sub>3</sub>H]Cl are shown in Fig. 11. [Zr-UiO-66-PDC-SO<sub>3</sub>H]Cl can be separated by centrifugation and reused without significantly reducing its catalytic reactivity. For this purpose, the recyclability of the catalyst was studied on the reaction of 4-chlorobenzaldehyde (1.0 mmol, 0.14 g), 2-aminoprop-1-ene-1,1,3-tricarbonitrile (1.0 mmol, 0.132 g), and malononitrile (1.1 mmol, 0.072 g) as a model reaction under the above mentioned optimized reaction conditions. The results show that [Zr-UiO-66-PDC-SO<sub>3</sub>H]Cl can be reused up to six times without noticeable changes in its catalytic activity. To

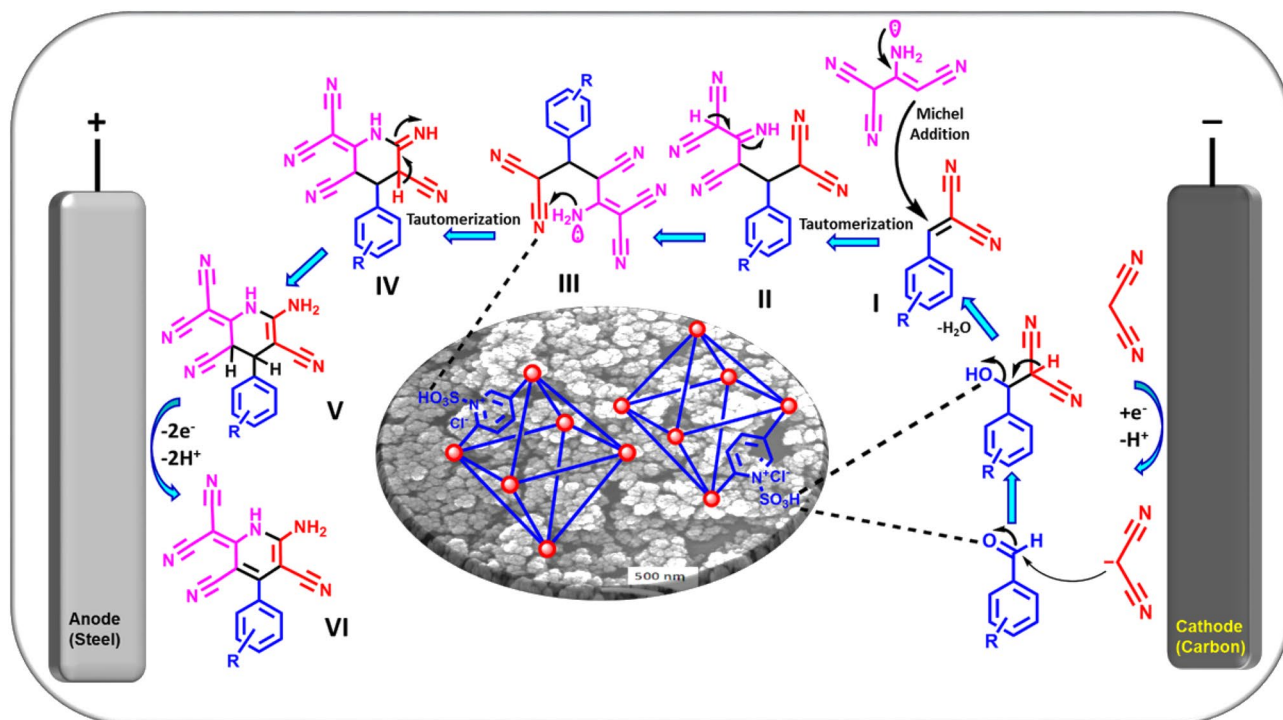


**Figure 10.** Convergent paired electrochemical synthesis of dicyanomethylene pyridine compounds.

Substrate	Current density (mA cm <sup>-2</sup> )	Isolated yield (%)
4-Chlorobenzaldehyde	0.5	35
4-Chlorobenzaldehyde	1.0	85
4-Chlorobenzaldehyde	1.5	25

**Table 3.** Optimization of conditions for the synthesis of dicyanomethylene pyridine.

confirm the above results, [Zr-UiO-66-PDC-SO<sub>3</sub>H]Cl was also analyzed by XRD and FT-IR spectra after its use in the reaction. These spectra were same as those of the fresh catalyst (Fig. 11).

## Conclusions

In this study, we have introduced a novel Zr-metal-organic frameworks [Zr-UiO-66-PDC-SO<sub>3</sub>H]Cl as a mesoporous catalyst. This catalyst was tested for the preparation of various novel dicyanomethylene pyridine via a cooperative vinyllogous anomeric based oxidation mechanism. The topology of the [Zr-UiO-66-PDC-SO<sub>3</sub>H]Cl was also characterized by SEM and TEM images. As well as, the thermal and solvent stability of the catalyst is high after the reaction of SO<sub>3</sub>HCl with [Zr-UiO-66-PDC]. Furthermore, the major advantages of the presented work are mild and green conditions, high yields, short reaction times, facile workup and reusability of the described [Zr-UiO-66-PDC-SO<sub>3</sub>H]Cl. Also, this paper provides a green and promising electrochemical procedure for the preparation of mesoporous (UiO-66-PDC). From the standpoint of environmental issues, synthesis of these compounds can be performed without the need for any ex-situ chemical agent such as a base or probase. On the other hands, the use of electricity eliminates the need for high temperature and pressure, which is the most outstanding features of this study. Furthermore, the convergent paired electrosynthesis of dicyanomethylene pyridine derivatives with the prepared catalyst was performed as an environmentally friendly technique under green conditions, at room temperature and pressure. We think that the present work is a promising insight for inter and multidisciplinary research, rational design, syntheses and applications of task-specific MOFs and bioactive molecules.

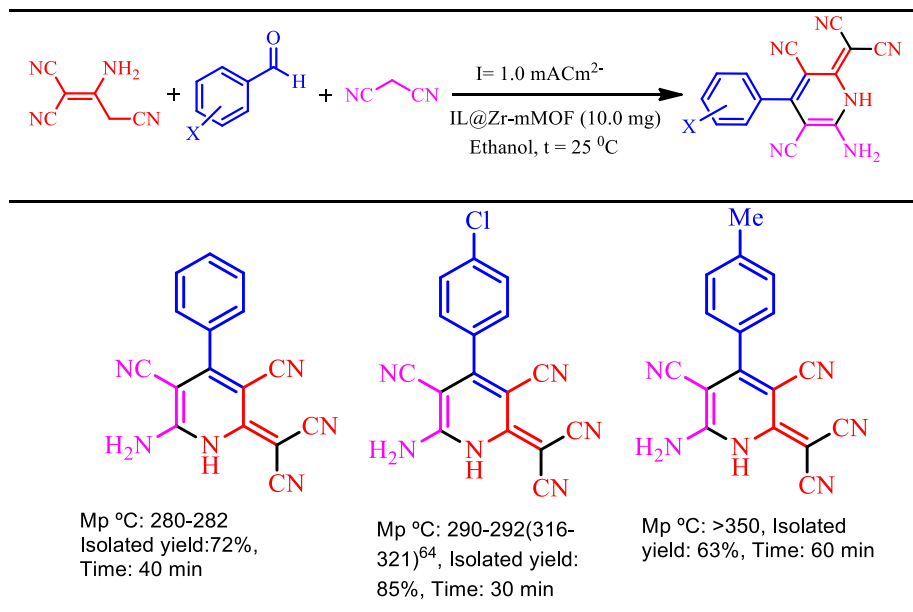


**Table 4.** Electrochemical synthesis of dicyanomethylene pyridine derivatives in the presence of [Zr-UiO-66-PDC-SO<sub>3</sub>H]Cl as a catalyst. At  $I = 1.0 \text{ mA cm}^{-2}$ .

Entry	Catalyst	(mol%)	Time (min)	Yield <sup>a</sup> (%)
1	SSA	10.0 mg	120	Trace
2	H <sub>2</sub> SO <sub>4</sub>	10	120	20
3	Fe <sub>3</sub> O <sub>4</sub>	10.0 mg	120	18
4	<i>p</i> -TSA	10	120	-
5	[PVI-SO <sub>3</sub> H]Cl	10.0 mg	120	43
6	MIL-100(Cr)/NHEtN(CH <sub>2</sub> PO <sub>3</sub> H <sub>2</sub> ) <sub>2</sub>	10.0 mg	120	56
7	Trichloroisocyanuric acid	10	120	-
8	Al(HSO <sub>4</sub> ) <sub>3</sub>	10	120	-
9	Mg(NO <sub>3</sub> ) <sub>2</sub> ·6H <sub>2</sub> O	10	120	28
10	NaHSO <sub>4</sub>	10	120	-
11	NH <sub>4</sub> NO <sub>3</sub>	10	120	-
12	FeCl <sub>3</sub>	10	120	38
13	H <sub>3</sub> [p(Mo <sub>3</sub> O <sub>10</sub> ) <sub>4</sub> ]·XH <sub>2</sub> O	10	120	-
14	Zn(NO <sub>3</sub> ) <sub>2</sub> ·6H <sub>2</sub> O	10	120	25
15	KOH	10	120	Trace
16	This work (Method A)	10	20	87

**Table 5.** Evaluation of various catalysts for the synthesis of dicyanomethylene pyridine in comparison with [Zr-UiO-66-PDC-SO<sub>3</sub>H]Cl. <sup>a</sup>Isolated yield.

## Materials and methods

Pyridine-2,5-dicarboxylic acid (H<sub>2</sub>PDC) (Merck, 95%), Zirconium tetrachloride (ZrCl<sub>4</sub>) (Sigma Aldrich, 98%), Potassium Nitrate (KNO<sub>3</sub>) (Sigma-Aldrich, 99%), formic acid (HCOOH) (Merck, 37%), Ethanol (C<sub>2</sub>H<sub>5</sub>OH) (Merck, 99%), Lithium Perchlorate (LiClO<sub>4</sub>) (Merck, 99%) and other materials (Merck) were reagent-grade materials and used as received without further purification. All solutions were prepared at room temperature. The

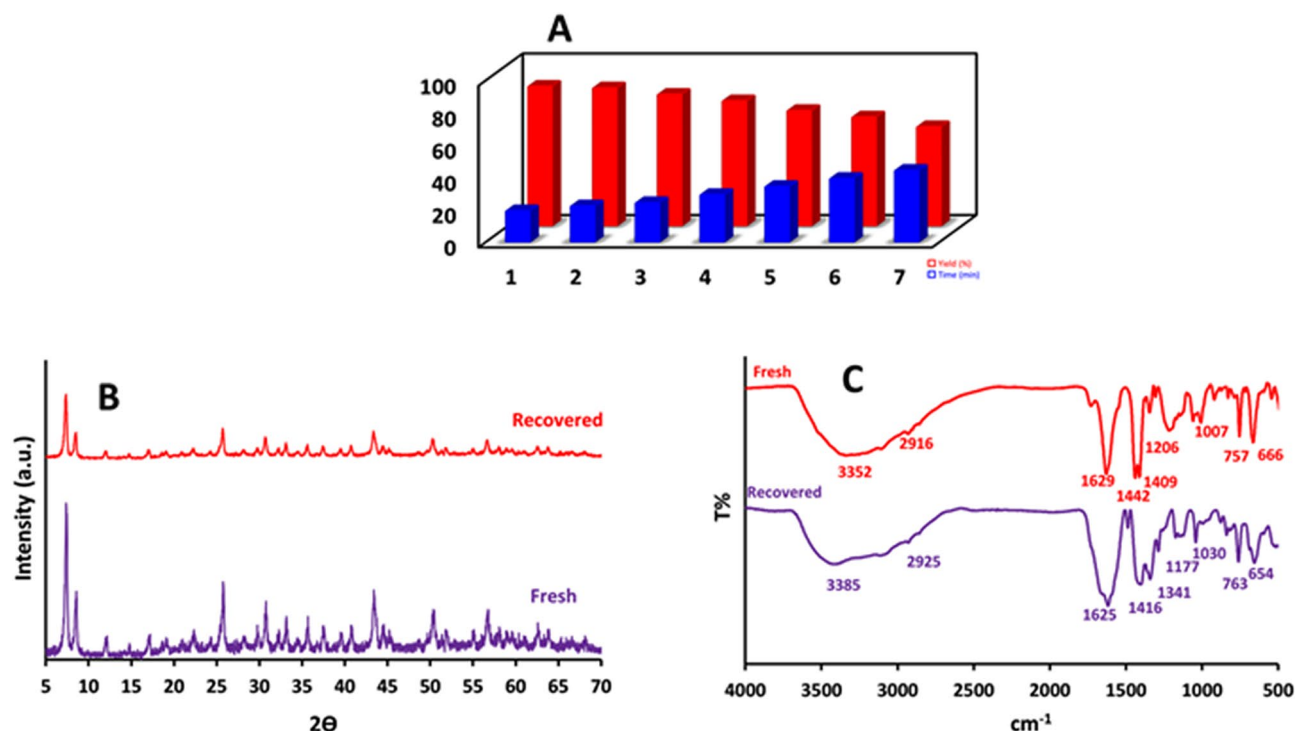


**Figure 11.** (A) Recyclability of [Zr-UiO-66-PDC-SO<sub>3</sub>H]Cl at the synthesis (2-methyl-1*H*-indol-3-yl)-pyrazolo[3,4-*b*]pyridine derivatives. (B,C) The characterization of reused catalysts after six runs using PXRD and FT-IR spectra.

known products were identified by comparison of their melting points and spectral data with those reported in the literature. To scrutinize the progress of the reaction, silica gel SIL G/UV 254 plates were used. From the model of the BRUKER Ultrashield FT-NMR spectrometer ( $\delta$  in ppm) were recorded <sup>1</sup>H NMR (600 or 400 MHz) and <sup>13</sup>C NMR (151 or 101 MHz). Recorded on a Büchi B-545 apparatus in open capillary tubes were melting points. The PerkinElmer PE-1600-FTIR device was recorded for infrared spectra of compounds. SEM was performed using a scanning electron microscope for field publishing made by TE-SCAN. Thermal gravimetry (TG), differential thermal gravimetric (DTG) and differential thermal (DTA) were analyzed by a Perkin Elmer (Model: Pyris 1). BET and BJH were analyzed by BELSORP-mini ii high precision Surface area and pore size.

**Electrosynthesis setup.** Electrosynthesis of catalyst and dicyanomethylene pyridine compounds were performed in a homemade undivided two-electrode cell. The cell consists of a cap glass bottle containing a precursor solution, carbon plate as working electrode (100 mm × 20 mm × 5 mm) and the U-shape stainless steel sheet as the auxiliary electrode. All of the electrochemical synthesis experiments were done at room temperature and pressure. Electrosynthesis of [Zr-UiO-66-PDC-SO<sub>3</sub>H]Cl and dicyanomethylene pyridine derivatives were accomplished by applying a suitable current density for a specified period.

**Chemical procedure for the preparation of Zr-UiO-66-PDC.** In a 100 mL round-bottomed flask, a mixture of pyridine-2,5-dicarboxylic acid (H<sub>2</sub>PDC) (0.366 g, 2.2 mmol) and ZrCl<sub>4</sub> (0.512 g, 2.2 mmol) with formic acid and H<sub>2</sub>O (9:1) 50 mL as solvent were stirred at 120 °C for 3 h under reflux conditions<sup>13</sup>. After this time, the suspension was filtered by centrifugation (2000 rpm, 20 min). Then, to the sediment was added H<sub>2</sub>O which was separated by centrifugation (2000 rpm, 20 min, 3 runs). Finally, a white precipitate was dried under a powerful vacuum at 90 °C to give Zr-UiO-66-PDC (Fig. 12).

**General procedure for the preparation of [Zr-UiO-66-PDC-SO<sub>3</sub>H]Cl.** In a 50 mL round-bottomed flask, a mixture of Zr-UiO-66-PDC (1.0 mmol, 0.282 g) and chlorosulfonic acid (1.0 mmol, 0.067 mL) in dry CH<sub>2</sub>Cl<sub>2</sub> (20.0 mL) at 0 °C were stirred for 2 h. Then, the sediment appeared which was filtered by centrifugation (1000 rpm, 5 min, 2 times) and dried under vacuum to obtain white precipitated as [Zr-UiO-66-PDC-SO<sub>3</sub>H]Cl (Fig. 12).

**Chemical procedure for the preparation of dicyanomethylene pyridine derivatives using [Zr-UiO-66-PDC-SO<sub>3</sub>H]Cl as an efficient catalyst.** In a 15 mL round-bottomed flask, a mixture of aldehyde (1.0 mmol, 0.398 g), 2-aminoprop-1-ene-1,1,3-tricarbonitrile (1.0 mmol, 0.132 g) and malononitrile (1.1 mmol, 0.073 g) and [Zr-UiO-66-PDC-SO<sub>3</sub>H]Cl (10.0 mg) as catalyst was stirred under solvent-free conditions at 100 °C. After completion of the reaction which was followed by TLC (*n*-hexane: ethyl acetate; 7:3), the

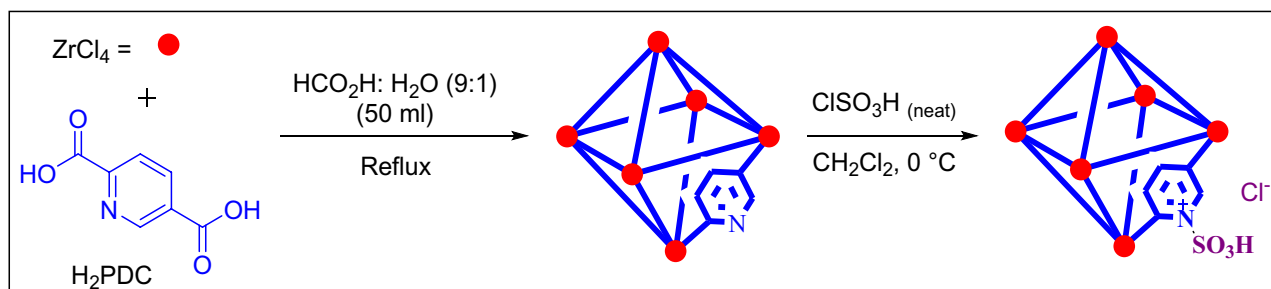


**Figure 12.** Chemical synthesis of [Zr-UiO-66-PDC-SO<sub>3</sub>H]Cl as a functionalized MOF catalyst.

reaction mixture was cool down to room temperature. Then, the mixture was added 10 mL ethanol and the catalyst was subsequently removed by centrifugation (1000 rpm). Finally, the product was recrystallized with EtOH (Fig. 2).

**Electrochemical procedure for the preparation of Zr-UiO-66-PDC.** In a typical procedure, (0.512 g, 2.2 mmol) of zirconium tetrachloride as a cation source, (0.366 g, 2.2 mmol) of pyridine-2,5-dicarboxylic acid (H<sub>2</sub>PDC) as ligand and (0.127 g, 0.1 mmol) potassium nitrate (KNO<sub>3</sub>) as a supporting electrolyte were dissolved in the 50.0 mL aqueous solution of formic acid (H<sub>2</sub>O/formic acid; 1/9). The solution was stirred at room temperature for 30 min before the electrolysis (30 mA cm<sup>-2</sup> for 1800s). After electrolysis, the solution was centrifuged at 5000 rpm for 5 min, and the precipitate was washed twice with distilled water and ethanol. The final MOF was then aged overnight at 100 °C.

**Electrochemical procedure for convergent paired electrosynthesis of dicyanomethylene pyridines.** The convergent paired electrosynthesis of dicyanomethylene pyridines derivatives was carried out in 50 mL of ethanol containing aldehyde derivatives (1.0 mmol), malononitrile (0.066 g, 1.0 mmol), 2-aminoprop-1-ene-1,1,3-tricarbonitrile (0.132 g, 1.0 mmol) and [Zr-UiO-66-PDC-SO<sub>3</sub>H]Cl (10.0 mg) as catalyst under stirring at 1.0 mA cm<sup>-2</sup>. The progress of the reaction was followed by thin-layer chromatography (*n*-hexane; ethylacetate). Also, the final product was separated by large scale thin-layer chromatography on the silica gel plate.

**Characteristic of the products.** *6-Amino-2-(dicyanomethylene)-4-phenyl-1,2-dihydropyridine-3,5-dicarbonitrile (1a).* Yellow solid; Mp: 280–283 °C; IR (KBr):  $\nu$  (cm<sup>-1</sup>) = 3374, 3306, 3215, 2218, 2191, 1642. <sup>1</sup>H NMR (400 MHz, DMSO-*d*<sub>6</sub>)  $\delta$  7.80 (s, 3H), 7.60–7.53 (m, 3H), 7.48 (d, *J* = 1.3 Hz, 2H). <sup>13</sup>C NMR (101 MHz, DMSO-*d*<sub>6</sub>)  $\delta$  160.5, 160.4, 157.8, 135.3, 129.7, 128.4, 128.3, 116.2, 115.9, 85.4, 80.7, 43.6 (See SI).

*6-Amino-4-(4-chlorophenyl)-2-(dicyanomethylene)-1,2-dihydropyridine-3,5-dicarbonitrile (2a).* Yellow solid; Mp: 290–262 °C; IR (KBr):  $\nu$  (cm<sup>-1</sup>) = 3363, 3302, 3211, 2228, 2217, 2191, 1645. <sup>1</sup>H NMR (600 MHz, DMSO-*d*<sub>6</sub>)  $\delta$  7.59 (d, *J* = 8.4 Hz, 2H), 7.46 (d, *J* = 8.4 Hz, 2H), 6.52 (s, 3H). <sup>13</sup>C NMR (151 MHz, DMSO-*d*<sub>6</sub>)  $\delta$  161.6, 159.5, 158.5, 134.9, 134.9, 130.8, 129.1, 116.8, 116.5, 85.6, 81.0, 44.2 (See SI).

*6-Amino-2-(dicyanomethylene)-4-(*p*-tolyl)-1,2-dihydropyridine-3,5-dicarbonitrile (3a).* Yellow solid; Mp: > 350 °C; IR (KBr):  $\nu$  (cm<sup>-1</sup>) = 3483, 3371, 3202, 2213, 2200, 2171, 1620. <sup>1</sup>H NMR (400 MHz, DMSO-*d*<sub>6</sub>)  $\delta$  7.29 (s, 4H), 6.87 (s, 2H), 2.38 (s, 3H). <sup>13</sup>C NMR (101 MHz, DMSO-*d*<sub>6</sub>)  $\delta$  162.7, 159.7, 158.7, 139.0, 132.8, 128.9, 128.3, 116.9, 116.6, 85.0, 80.3, 20.9 (See SI).

*6-Amino-2-(dicyanomethylene)-4-(3-nitrophenyl)-1,2-dihydropyridine-3,5-dicarbonitrile (4a).* Yellow solid; Mp: 316–318 °C; IR (KBr):  $\nu$  (cm<sup>-1</sup>) = 3438, 3339, 3213, 2197, 2181, 1657, 1556, 1352. <sup>1</sup>H NMR (600 MHz, DMSO-*d*<sub>6</sub>)  $\delta$  8.38–8.35 (m, 1H), 8.33–8.30 (m, 1H), 7.93 (d, *J* = 7.7 Hz, 1H), 7.83 (t, *J* = 8.0 Hz, 1H), 7.05 (s, 2H). <sup>13</sup>C NMR (151 MHz, DMSO-*d*<sub>6</sub>)  $\delta$  163.0, 159.0, 157.9, 148.0, 137.8, 135.9, 130.8, 124.8, 123.9, 117.1, 116.9, 85.3, 80.7, 44.3 (See SI).

*6-Amino-2-(dicyanomethylene)-4-(4-hydroxyphenyl)-1,2-dihydropyridine-3,5-dicarbonitrile (5a).* Yellow solid; Mp: > 350 °C; IR (KBr):  $\nu$  (cm<sup>-1</sup>) = 3342, 3227, 2183, 1652, 1553. <sup>1</sup>H NMR (600 MHz, DMSO-*d*<sub>6</sub>)  $\delta$  9.85 (s, 1H), 7.23 (d, *J* = 8.5 Hz, 2H), 6.89–6.78 (m, 4H). <sup>13</sup>C NMR (151 MHz, DMSO-*d*<sub>6</sub>)  $\delta$  163.4, 160.1, 159.3, 159.1, 130.6, 126.6, 117.7, 117.3, 115.5, 85.6, 80.7, 43.6 (See SI).

*6-Amino-2-(dicyanomethylene)-4-(4-nitrophenyl)-1,2-dihydropyridine-3,5-dicarbonitrile (6a).* Yellow solid; Mp: > 350 °C; IR (KBr):  $\nu$  (cm<sup>-1</sup>) = 3336, 2196, 1655, 1556, 1508, 1360. <sup>1</sup>H NMR (600 MHz, DMSO-*d*<sub>6</sub>)  $\delta$  8.35 (d, *J* = 8.7 Hz, 2H), 7.74 (d, *J* = 8.7 Hz, 2H), 7.05 (s, 2H). <sup>13</sup>C NMR (151 MHz, DMSO-*d*<sub>6</sub>)  $\delta$  162.9, 159.0, 158.3, 148.5, 142.9, 130.7, 124.1, 116.9, 116.7, 85.0, 80.4, 44.3 (See SI).

*6-Amino-4-(2-chlorophenyl)-2-(dicyanomethylene)-1,2-dihydropyridine-3,5-dicarbonitrile (7a).* Yellow solid; Mp: > 350 °C; IR (KBr):  $\nu$  (cm<sup>-1</sup>) = 3438, 3342, 3231, 2195, 2164, 1636, 1557. <sup>1</sup>H NMR (600 MHz, DMSO-*d*<sub>6</sub>)  $\delta$

7.61 (dd,  $J=7.9, 1.3$  Hz, 1H), 7.50 (td,  $J=7.7, 1.9$  Hz, 1H), 7.47 (td,  $J=7.5, 1.4$  Hz, 1H), 7.40 (dd,  $J=7.4, 1.8$  Hz, 1H), 7.00 (s, 2H).  $^{13}\text{C}$  NMR (151 MHz, DMSO- $d_6$ )  $\delta$  162.7, 158.9, 157.9, 135.5, 131.6, 131.4, 130.7, 130.0, 128.0, 116.6, 116.3, 86.0, 81.1, 44.0 (See SI).

**6-Amino-2-(dicyanomethylene)-4-(3-ethoxy-4-hydroxyphenyl)-1,2-dihydropyridine-3,5-dicarbonitrile (8a).** Yellow solid; Mp: 333–335 °C; IR (KBr):  $\nu$  ( $\text{cm}^{-1}$ ) = 3431, 3342, 3236, 2198, 1665, 1649, 1554.  $^1\text{H}$  NMR (600 MHz, DMSO- $d_6$ )  $\delta$  9.38 (s, 1H), 6.97 – 6.94 (m, 1H), 6.87 (d,  $J=8.1$  Hz, 1H), 6.85 – 6.78 (m, 3H), 4.06 (q,  $J=7.0$  Hz, 2H), 1.36 – 1.33 (m, 3H).  $^{13}\text{C}$  NMR (151 MHz, DMSO- $d_6$ )  $\delta$  163.3, 160.1, 159.3, 148.6, 146.5, 126.8, 122.1, 117.8, 117.4, 115.7, 114.6, 85.6, 80.8, 64.3, 43.6, 15.1 (See SI).

**6-Amino-2-(dicyanomethylene)-1,2-dihydro-[4,4'-bipyridine]-3,5-dicarbonitrile (9a).** Yellow solid; Mp: > 350 °C; IR (KBr):  $\nu$  ( $\text{cm}^{-1}$ ) = 3443, 3345, 3224, 2211, 2195, 2175, 1650, 1569.  $^1\text{H}$  NMR (600 MHz, DMSO- $d_6$ )  $\delta$  8.72 (d,  $J=5.7$  Hz, 2H), 7.46 (d,  $J=4.4$  Hz, 2H), 7.04 (s, 2H).  $^{13}\text{C}$  NMR (151 MHz, DMSO- $d_6$ )  $\delta$  162.9, 159.0, 157.7, 150.3, 144.2, 123.6, 116.9, 116.6, 84.7, 80.1, 44.3 (See SI).

**6-Amino-2-(dicyanomethylene)-4-(thiophen-2-yl)-1,2-dihydropyridine-3,5-dicarbonitrile (10a).** Yellow solid; Mp: > 350 °C; IR (KBr):  $\nu$  ( $\text{cm}^{-1}$ ) = 3481, 3345, 3211, 2213, 2189, 2163, 1624, 1555.  $^1\text{H}$  NMR (600 MHz, DMSO- $d_6$ )  $\delta$  7.82 (d,  $J=4.9$  Hz, 1H), 7.37 (d,  $J=3.5$  Hz, 1H), 7.23 – 7.18 (m, 1H), 6.97 (s, 2H).  $^{13}\text{C}$  NMR (151 MHz, DMSO- $d_6$ )  $\delta$  163.4, 159.3, 152.2, 135.2, 130.4, 129.6, 127.9, 117.3, 116.9, 85.8, 81.0, 44.2 (See SI).

**6-Amino-2-(dicyanomethylene)-4-(2-nitrophenyl)-1,2-dihydropyridine-3,5-dicarbonitrile (11a).** Yellow solid; Mp: > 350 °C; IR (KBr):  $\nu$  ( $\text{cm}^{-1}$ ) = 3437, 3341, 3230, 2218, 2195, 1637, 1560, 1517, 1351.  $^1\text{H}$  NMR (600 MHz, DMSO- $d_6$ )  $\delta$  8.27 (d,  $J=8.2$  Hz, 1H), 7.92 (t,  $J=7.5$  Hz, 1H), 7.80 (t,  $J=7.9$  Hz, 1H), 7.60 (d,  $J=7.5$  Hz, 1H), 7.05 (s, 2H).  $^{13}\text{C}$  NMR (151 MHz, DMSO- $d_6$ )  $\delta$  170.8, 162.6, 158.8, 158.1, 147.3, 135.2, 131.8, 131.6, 131.3, 125.4, 116.6, 116.4, 84.9, 80.2, 60.2, 44.1, 21.2, 14.6 (See SI).

**6-Amino-2-(dicyanomethylene)-4-(3,4-dihydroxyphenyl)-1,2-dihydropyridine-3,5-dicarbonitrile (12a).** Yellow solid; Mp: > 350 °C; IR (KBr):  $\nu$  ( $\text{cm}^{-1}$ ) = 3457, 3334, 3225, 2197, 2168, 1650, 1560.  $^1\text{H}$  NMR (600 MHz, DMSO- $d_6$ )  $\delta$  9.33 (s, 1H), 9.26 (s, 1H), 6.80 (d,  $J=8.0$  Hz, 3H), 6.77 (s, 1H), 6.67 (d,  $J=8.1$  Hz, 1H) (See SI).

**6-Amino-2-(dicyanomethyl)-4-(3,4-dimethoxyphenyl)-1,2-dihydropyridine-3,5-dicarbonitrile (13a).** Yellow solid; Mp: 332–335 °C; IR (KBr):  $\nu$  ( $\text{cm}^{-1}$ ) = 3504, 3489, 3374, 2216, 2194, 2172, 1613, 1551.  $^1\text{H}$  NMR (400 MHz, DMSO- $d_6$ )  $\delta$  7.07 (d,  $J=8.3$  Hz, 1H), 7.03 (d,  $J=2.1$  Hz, 1H), 6.97 (dd,  $J=8.2, 2.1$  Hz, 1H), 6.88 (s, 2H), 3.82 (s, 3H), 3.79 (s, 3H).  $^{13}\text{C}$  NMR (101 MHz, DMSO- $d_6$ )  $\delta$  162.7, 159.3, 158.8, 149.6, 148.0, 127.7, 121.3, 117.1, 116.7, 112.2, 111.2, 85.1, 80.3, 55.5, 55.4, 43.1, 40.0 (See SI).

**6'-Amino-2'-(dicyanomethylene)-1',2'-dihydro-[3,4'-bipyridine]-3',5'-dicarbonitrile (14a).** Brown solid; Mp: > 350 °C; IR (KBr):  $\nu$  ( $\text{cm}^{-1}$ ) = 3389, 3317, 3161, 2209, 2189, 2156, 1654, 1577, 1514.  $^1\text{H}$  NMR (400 MHz, DMSO- $d_6$ )  $\delta$  8.79 – 8.47 (m, 2H), 7.91 (dt,  $J=7.9, 2.0$  Hz, 1H), 7.55 (dd,  $J=7.9, 4.9$  Hz, 1H), 7.03 (s, 2H).  $^{13}\text{C}$  NMR (101 MHz, DMSO- $d_6$ )  $\delta$  162.52, 158.57, 156.38, 150.38, 148.47, 136.39, 131.89, 123.40, 116.65, 116.43, 85.08, 80.40, 40.03 (See SI).

**6-Amino-4-(4-bromophenyl)-2-(dicyanomethylene)-1,2-dihydropyridine-3,5-dicarbonitrile (15a).** White solid; Mp: 330–332 °C; IR (KBr):  $\nu$  ( $\text{cm}^{-1}$ ) = 3451, 3339, 3224, 2214, 2194, 2170, 1674, 1572, 1511.  $^1\text{H}$  NMR (400 MHz, DMSO- $d_6$ )  $\delta$  7.77 – 7.64 (m, 2H), 7.46 – 7.30 (m, 2H), 6.97 (s, 2H).  $^{13}\text{C}$  NMR (101 MHz, DMSO- $d_6$ )  $\delta$  162.5, 158.5, 158.5, 135.0, 131.4, 130.6, 123.0, 116.7, 116.4, 84.8, 80.1, 40.0 (See SI).

**6-Amino-2-(dicyanomethylene)-4-(3-hydroxyphenyl)-1,2-dihydropyridine-3,5-dicarbonitrile (16a).** Yellow solid; Mp: > 350 °C; IR (KBr):  $\nu$  ( $\text{cm}^{-1}$ ) = 3476, 3330, 3218, 2202, 2171, 1625, 1548.  $^1\text{H}$  NMR (600 MHz, DMSO- $d_6$ )  $\delta$  9.72 (s, 1H), 7.28 (t,  $J=7.8$  Hz, 1H), 6.94 – 6.84 (m, 3H), 6.77 (d,  $J=7.5$  Hz, 1H), 6.73 (s, 1H) (See SI).

**6-Amino-2-(dicyanomethylene)-4-(4-fluorophenyl)-1,2-dihydropyridine-3,5-dicarbonitrile (17a).** Yellow solid; Mp: 324–326 °C; IR (KBr):  $\nu$  ( $\text{cm}^{-1}$ ) = 3449, 3374, 3309, 3216, 2212, 2194, 2171, 1646.  $^1\text{H}$  NMR (600 MHz, DMSO- $d_6$ )  $\delta$  7.51 – 7.45 (m, 2H), 7.34 (t,  $J=8.6$  Hz, 2H), 6.97 (s, 2H) (See SI).

**4,4',4''-(((1,3,5-Triazine-2,4,6-triyl)tris(oxy))tris(benzene-4,1-diyl))tris(6-amino-2-(dicyanomethylene)-1,2-dihydropyridine-3,5-dicarbonitrile) (18a).** Yellow solid; Mp: > 350 °C; IR (KBr):  $\nu$  ( $\text{cm}^{-1}$ ) = 3504, 3374, 3224, 2215, 2194, 2166, 1613, 1551.  $^1\text{H}$  NMR (400 MHz, DMSO- $d_6$ )  $\delta$  7.53 (td,  $J=8.5, 4.3$  Hz, 1H), 7.49 – 7.41 (m, 2H), 7.38 (d,  $J=8.6$  Hz, 1H), 6.95 (s, 1H), 6.91 (s, 1H).  $^{13}\text{C}$  NMR (101 MHz, DMSO- $d_6$ )  $\delta$  173.3, 163.2, 159.2, 159.1, 153.2, 152.5, 133.9, 132.5, 130.6, 130.1, 122.0, 121.7, 120.6, 117.3, 117.0, 85.5, 80.8, 40.5, 40.3, 40.1 (See SI).

**4,4'-(1,4-Phenylene)bis(6-amino-2-(dicyanomethylene)-1,2-dihydropyridine-3,5-dicarbonitrile) (19a).** Yellow solid; Mp: > 350 °C; IR (KBr):  $\nu$  ( $\text{cm}^{-1}$ ) = 3395, 3334, 3228, 2192, 2158, 1650, 1549, 1429.  $^1\text{H}$  NMR (400 MHz, DMSO- $d_6$ )  $\delta$  7.55 (s, 1H), 6.94 (s, 1H).  $^{13}\text{C}$  NMR (101 MHz, DMSO- $d_6$ )  $\delta$  159.2, 144.3, 139.6, 135.2, 135.0, 134.8, 132.4, 131.5, 129.1, 128.9, 126.5, 126.4, 121.7, 121.2, 120.1, 119.6, 118.4, 116.8, 111.1, 111.0, 110.8, 102.8, 42.3 (See SI).



Received: 16 April 2021; Accepted: 3 August 2021

Published online: 19 August 2021

## References

- Makal, T. A., Li, J.-R., Lu, W. & Zhou, H.-C. Methane storage in advanced porous materials. *Chem. Soc. Rev.* **41**, 7761–7779 (2012).
- Davis, M. E. Ordered porous materials for emerging applications. *Nature* **417**, 813–821 (2002).
- Ariga, K., Ito, H., Hill, J. P. & Tsukube, H. Molecular recognition: From solution science to nano/materials technology. *Chem. Soc. Rev.* **41**, 5800–5835 (2012).
- Yamauchi, Y., Suzuki, N., Radhakrishnan, L. & Wang, L. Breakthrough and future: Nanoscale controls of compositions, morphologies, and mesochannel orientations toward advanced mesoporous materials. *Chem. Rec.* **9**, 321–339 (2009).
- Fujie, K. & Kitagawa, H. Ionic liquid transported into metal–organic frameworks. *Coord. Chem. Rev.* **307**, 382–390 (2016).
- Sarker, M., An, H. J., Yoo, D. K. & Jhung, S. H. Nitrogen-doped porous carbon from ionic liquid@ Al-metal-organic framework: A prominent adsorbent for purification of both aqueous and non-aqueous solutions. *Chem. Eng. J.* **338**, 107–116 (2018).
- Cavka, J. H. *et al.* A new zirconium inorganic building brick forming metal organic frameworks with exceptional stability. *J. Am. Chem. Soc.* **130**, 13850–13851 (2008).
- Li, M., Li, D., O’Keeffe, M. & Yaghi, O. M. Topological analysis of metal–organic frameworks with polytopic linkers and/or multiple building units and the minimal transitivity principle. *Chem. Rev.* **114**, 1343–1370 (2014).
- Bai, Y. *et al.* Zr-based metal–organic frameworks: Design, synthesis, structure, and applications. *Chem. Soc. Rev.* **45**, 2327–2367 (2016).
- Schaate, A. *et al.* Modulated synthesis of Zr-based metal–organic frameworks: From nano to single crystals. *Chem.-Eur. J.* **17**, 6643–6651 (2011).
- Bueken, B. *et al.* A zirconium squarate metal–organic framework with modulator-dependent molecular sieving properties. *Chem. Commun.* **50**, 10055–10058 (2014).
- Wang, H. *et al.* Topologically guided tuning of Zr-MOF pore structures for highly selective separation of C6 alkane isomers. *Nat. Commun.* **9**, 1–11 (2018).
- Waitschat, S. *et al.* Synthesis of M-UiO-66 (M= Zr, Ce or Hf) employing 2, 5-pyridinedicarboxylic acid as a linker: Defect chemistry, framework hydrophilisation and sorption properties. *Dalton Trans.* **47**, 1062–1070 (2018).
- Zolfigol, M. A., Khakyzadeh, V., Shirmardi, B., Moosavi-Zare, A. R. & Zare, A. Ionic liquid 3-methyl-1-sulfonic acid imidazolium chloride ([Msim]Cl): A new and highly efficient catalyst for the synthesis of 1–1, 8-dioxo-decahydroacridine derivatives with antibacterial properties. *Clin. Biochem.* **13**, S55 (2011).
- Zarei, M. Spotlight:[Msim] X: As a versatile catalyst and reagent. *Iran. J. Catal.* **8**, 237–240 (2018).
- Moosavi-Zare, A. R. *et al.* Design, characterization and application of new ionic liquid 1-sulfolpyridinium chloride as an efficient catalyst for tandem Knoevenagel–Michael reaction of 3-methyl-1-phenyl-1H-pyrazol-5 (4H)-one with aldehydes. *Appl. Catal. A* **467**, 61–68 (2013).
- Babae, S., Zolfigol, M. A., Zarei, M., Abbasi, M. & Najafi, Z. Synthesis of pyridinium-based salts: Catalytic application at the synthesis of six membered O-heterocycles. *Mol. Catal.* **475**, 110403 (2019).
- Moosavi-Zare, A. R., Zolfigol, M. A., Zarei, M., Noroozizadeh, E. & Beyzavi, M. H. Nitration of arenes by 1-sulfolpyridinium nitrate as an ionic liquid and reagent by in situ generation of NO<sub>2</sub>. *RSC Adv.* **6**, 89572–89577 (2016).
- Moradi, S. *et al.* An efficient catalytic method for the synthesis of pyrido [2, 3-d] pyrimidines as biologically drug candidates by using novel magnetic nanoparticles as a reusable catalyst. *Appl. Organomet. Chem.* **32**, e4043 (2018).
- Babae, S., Zolfigol, M. A., Zarei, M. & Zamanian, J. 1, 10-Phenanthroline-based molten salt as a bifunctional sulfonic acid catalyst: Application to the synthesis of N-heterocycle compounds via anomeric based oxidation. *ChemistrySelect* **3**, 8947–8954 (2018).
- Pedrosa, L. F. *et al.* Synthesis and characterization of new 1H-pyrazolo [3, 4-b] pyridine phosphoramidate derivatives. *ARKIVOC* **4**, 38–50 (2014).
- Kumar, V., Kaur, K., Gupta, G. K. & Sharma, A. K. Pyrazole containing natural products: Synthetic preview and biological significance. *Eur. J. Med. Chem.* **69**, 735–753 (2013).
- Shi, D. Q., Yao, H. & Shi, J. W. Three-component, one-pot synthesis of Pyrazolo [3, 4-b] pyridine derivatives in aqueous media. *Synth. Commun.* **38**, 1662–1669 (2008).
- Eissa, I. H., El-Naggar, A. M. & El-Hashash, M. A. Design, synthesis, molecular modeling and biological evaluation of novel 1H-pyrazolo [3, 4-b] pyridine derivatives as potential anticancer agents. *Bioorg. Chem.* **67**, 43–56 (2016).
- El-Emary, T. I. Synthesis of newly substituted pyrazoles and substituted pyrazolo [3, 4-b] pyridines based on 5-amino-3-methyl-1-phenylpyrazole. *J. Chin. Chem. Soc.* **54**, 507–518 (2007).
- Zhang, X. *et al.* Controllable synthesis of pyrazolo [3, 4-b] pyridines or substituted malononitrile derivatives through multi-component reactions in ionic liquid. *Aust. J. Chem.* **62**, 382–388 (2009).
- Afsar, J. *et al.* Synthesis and application of a novel nanomagnetic catalyst with Cl[DABCO-NO<sub>2</sub>]C(NO<sub>2</sub>)<sub>3</sub> tags in the preparation of pyrazolo [3, 4-b] pyridines via anomeric based oxidation. *Res. Chem. Intermed.* **44**, 7595–7618 (2018).
- Alabugin, I. V. *Stereoelectronic Effects: A Bridge Between Structure and Reactivity* (Wiley, 2016).
- Alabugin, I. V., dos Passos Gomes, G. & Abdo, M. A. Hyperconjugation. *Wiley Interdiscip. Rev. Comput. Mol. Sci.* **9**, e1389 (2019).
- Karimi, F., Yarie, M. & Zolfigol, M. A. Synthesis and characterization of Fe<sub>3</sub>O<sub>4</sub>@ SiO<sub>2</sub>/(CH<sub>2</sub>)<sub>3</sub>NH(CH<sub>2</sub>)<sub>2</sub>O<sub>2</sub>P(OH)<sub>2</sub> and its catalytic application in the synthesis of benzo-[h] quinoline-4-carboxylic acids via a cooperative anomeric based oxidation mechanism. *Mol. Catal.* **489**, 110924 (2020).
- Afsar, J. *et al.* Synthesis and application of melamine-based nano catalyst with phosphonic acid tags in the synthesis of (3'-indolyl) pyrazolo [3, 4-b] pyridines via vinylogous anomeric based oxidation. *Mol. Catal.* **482**, 110666 (2020).
- Babae, S., Zarei, M., Sepehrmansourie, H., Zolfigol, M. A. & Rostamnia, S. Synthesis of metal-organic frameworks MIL-101(Cr)-NH<sub>2</sub> containing phosphorous acid functional groups: Application for the synthesis of N-Amino-2-pyridone and pyrano [2, 3-c] pyrazole derivatives via a cooperative vinylogous anomeric-based oxidation. *ACS Omega* **5**, 6240–6249 (2020).
- Jalili, F., Zarei, M., Zolfigol, M. A., Rostamnia, S. & Moosavi-Zare, A. R. SBA-15/PrN(CH<sub>2</sub>PO<sub>3</sub>H<sub>2</sub>)<sub>2</sub> as a novel and efficient mesoporous solid acid catalyst with phosphorous acid tags and its application on the synthesis of new pyrimido [4, 5-b] quinolones and pyrido [2, 3-d] pyrimidines via anomeric based oxidation. *Microporous Mesoporous Mater.* **294**, 109865 (2020).
- Ghasemi, P., Yarie, M., Zolfigol, M. A., Taherpour, A. A. & Torabi, M. Ionically Tagged magnetic nanoparticles with urea linkers: Application for preparation of 2-Aryl-quinoline-4-carboxylic acids via an anomeric-based oxidation mechanism. *ACS Omega* **5**, 3207–3217 (2020).
- Karimi, F., Yarie, M. & Zolfigol, M. A. A convenient method for synthesis of terpyridines via a cooperative vinylogous anomeric based oxidation. *RSC Adv.* **10**, 25828–25835 (2020).
- Dashteh, M. *et al.* Synthesis of cobalt tetra-2, 3-pyridiniumporphyrinato with sulfonic acid tags as an efficient catalyst and its application for the synthesis of bicyclic ortho-aminocarbonitriles, cyclohexa-1, 3-dienamines and 2-amino-3-cyanopyridines. *RSC Adv.* **10**, 27824–27834 (2020).

37. Yarie, M. Spotlight: Catalytic vinylogous anomeric based oxidation (Part I). *Iran. J. Catal.* **10**, 79–83 (2020).
38. Yarie, M. Catalytic anomeric based oxidation. *Iran. J. Catal. Spotlight* **7**, 85–88 (2017).
39. Alizadeh, S. & Nematollahi, D. Electrochemically assisted self-assembly technique for the fabrication of mesoporous metal–organic framework thin films: Composition of 3D hexagonally packed crystals with 2D honeycomb-like mesopores. *J. Am. Chem. Soc.* **139**, 4753–4761 (2017).
40. Alizadeh, S. & Nematollahi, D. convergent and Divergent paired electrodeposition of Metal-organic framework thin films. *Sci. Rep.* **9**, 1–13 (2019).
41. Wagner, A. *Preparation, Functionalization and Analysis of UiO-66 Metal-Organic Framework Thin Films on Silicon Photocathodes* (Uppsala University, 2015).
42. Li, M. & Dincă, M. On the Mechanism of MOF-5 Formation under Cathodic Bias. *Chem. Mater.* **27**, 3203–3206 (2015).
43. Li, M. & Dincă, M. Reductive electrosynthesis of crystalline metal–organic frameworks. *J. Am. Chem. Soc.* **133**, 12926–12929 (2011).
44. Campagnol, N. *et al.* On the electrochemical deposition of metal–organic frameworks. *J. Mater. Chem. A.* **4**, 3914–3925 (2016).
45. Soury, S., Bahrami, A., Alizadeh, S., Shahna, F. G. & Nematollahi, D. Development of a needle trap device packed with zinc based metal-organic framework sorbent for the sampling and analysis of polycyclic aromatic hydrocarbons in the air. *Microchem. J.* **148**, 346–354 (2019).
46. Firoozichahak, A. *et al.* UiO-66-NH<sub>2</sub> packed needle trap for accurate and reliable sampling and analysis of the halogenated volatile organic compounds in air. *Int. J. Environ. Anal. Chem.* **101**, 263–268 (2019).
47. Firoozichahak, A. *et al.* Development of a needle trap device packed with titanium based metal-organic framework sorbent for extraction of phenolic derivatives in air. *J. Sep. Sci.* **43**, 1011–1018 (2019).
48. Pirmohammadi, Z. *et al.* Determination of urinary methylhippuric acids using MIL-53-NH<sub>2</sub> (Al) metal–organic framework in microextraction by packed sorbent followed by HPLC–UV analysis. *Biomed. Chromatogr.* **34**, e4725 (2020).
49. Saedi, N. *et al.* A needle trap device packed with MIL-100 (Fe) metal organic frameworks for efficient headspace sampling and analysis of urinary BTEXs. *Biomed. Chromatogr.* **34**, e4800 (2020).
50. Langari, A. A. A., Firoozichahak, A., Alizadeh, S., Nematollahi, D. & Farhadian, M. Efficient extraction of aromatic amines in the air by the needle trap device packed with the zirconium based metal–organic framework sorbent. *RSC. Adv.* **10**, 13562–13572 (2020).
51. DeStefano, M. R., Islamoglu, T., Garibay, S. J., Hupp, J. T. & Farha, O. K. Room-temperature synthesis of UiO-66 and thermal modulation of densities of defect sites. *Chem. Mater.* **29**, 1357–1361 (2017).
52. Shearer, G. C. *et al.* Defect engineering: Tuning the porosity and composition of the metal–organic framework UiO-66 via modulated synthesis. *Chem. Mater.* **28**, 3749–3761 (2016).
53. Trickett, C. A. *et al.* Definitive molecular level characterization of defects in UiO-66 crystals. *Angew. Chem. Int. Ed.* **54**, 11162–11167 (2015).
54. Stassen, I. *et al.* Electrochemical film deposition of the zirconium metal–organic framework UiO-66 and application in a miniaturized sorbent trap. *Chem. Mater.* **27**, 1801–1807 (2015).
55. Wei, J.-Z. *et al.* Rapid and low-cost electrochemical synthesis of UiO-66-NH<sub>2</sub> with enhanced fluorescence detection performance. *Inorg. Chem.* **58**, 6742–6747 (2019).
56. Zhang, T. *et al.* Rapid synthesis of UiO-66 by means of electrochemical cathode method with electrochemical detection of 2, 4, 6-TCP. *Inorg. Chem. Commun.* **111**, 107671 (2020).
57. Momeni, S. & Nematollahi, D. New insights into the electrochemical behavior of acid orange 7: Convergent paired electrochemical synthesis of new aminonaphthol derivatives. *Sci. Rep.* **7**, 1–10 (2017).
58. Mokhtari, B., Nematollahi, D. & Salehzadeh, H. Paired electrochemical conversion of nitroarenes to sulfonamides, diarylsulfones and bis (arylsulfonyl) aminophenols. *Green Chem.* **20**, 1499–1505 (2018).
59. Jamshidi, M., Nematollahi, D., Taheri, F. & Alizadeh, H. Paired electrochemical method for synthesis of new phenylcarbonimidoyl dicyanide dyes. *Acs. Sustain. Chem. Eng.* **7**, 1956–1962 (2018).
60. Amatore, C. & Brown, A. R. Paired electrosynthesis at the femtomolar scale: Formation of 9, 10-Anthracenedione from the oxidation of Anthracene and reduction of dioxygen. *J. Am. Chem. Soc.* **118**, 1482–1486 (1996).
61. Frontana-Urbe, B. A., Little, R. D., Ibanez, J. G., Palma, A. & Vasquez-Medrano, R. Organic electrosynthesis: A promising green methodology in organic chemistry. *Green Chem.* **12**, 2099–2119 (2010).
62. Lorente, M. J., Nguyen, B. H., Kubiak, C. P. & Moeller, K. D. Paired electrolysis in the simultaneous production of synthetic intermediates and substrates. *J. Am. Chem. Soc.* **138**, 15110–15113 (2016).
63. Wu, T., Nguyen, B. H., Daugherty, M. C. & Moeller, K. D. Paired electrochemical reactions and the on-site generation of a chemical reagent. *Angew. Chem.* **131**, 3600–3603 (2019).
64. Fuentes, L. *et al.* Synthesis of heterocyclic compounds. Xxiii: Pyridines from malononitrile dimer and benzylidenemalononitriles. *Synthesis* **4**, 320–322 (1982).
65. Moustafa, M. S. *et al.* Unexpected behavior of enamines: Interesting new routes to 1, 6-naphthyridines, 2-oxopyrrolidines and pyrano [4, 3, 2-*de*][1, 6] naphthyridines. *Molecules* **18**, 276–286 (2013).
66. Katritzky, A. R., Steel, P. J. & Denisenko, S. N. X-Ray crystallographic evidence for a vinylogous anomeric effect in benzotriazole-substituted heterocycles. *Tetrahedron* **57**, 3309–3314 (2001).

## Acknowledgements

We thank Bu-Ali Sina University, Shanxi University (China) and Iran National Science Foundation (INSF) (98020070) for financial support to our research group.

## Author contributions

A.M.N., S.B. and M.Z.: methodology, validation, investigation, writing the original draft. M.A.Z.: supervision, resources, project administration, funding acquisition, conceptualization, writing-review. D.N. and S.A. writing-review & editing, supervision, project administration. J.A. and H.S. did some experiments.

## Competing interests

The authors declare no competing interests.

## Additional information

**Supplementary Information** The online version contains supplementary material available at <https://doi.org/10.1038/s41598-021-96001-7>.

**Correspondence** and requests for materials should be addressed to M.Z., S.A., M.A.Z. or D.N.

**Reprints and permissions information** is available at [www.nature.com/reprints](http://www.nature.com/reprints).

**Publisher's note** Springer Nature remains neutral with regard to jurisdictional claims in published maps and institutional affiliations.



**Open Access** This article is licensed under a Creative Commons Attribution 4.0 International License, which permits use, sharing, adaptation, distribution and reproduction in any medium or format, as long as you give appropriate credit to the original author(s) and the source, provide a link to the Creative Commons licence, and indicate if changes were made. The images or other third party material in this article are included in the article's Creative Commons licence, unless indicated otherwise in a credit line to the material. If material is not included in the article's Creative Commons licence and your intended use is not permitted by statutory regulation or exceeds the permitted use, you will need to obtain permission directly from the copyright holder. To view a copy of this licence, visit <http://creativecommons.org/licenses/by/4.0/>.

© The Author(s) 2021